npj regenerative medicine

www.nature.com/npjregenmed

ARTICLE OPEN

Check for updates

MAP4Ks inhibition promotes retinal neuron regeneration from Müller glia in adult mice

Houjian Zhang[1,2,3], Yuli Guo[1,2,3], Yaqiong Yang[1], Yuqian Wang[1], Youwen Zhang[1], Jingbin Zhuang[1], Yuting Zhang[1], Mei Shen[1], Jiankai Zhao[1], Rongrong Zhang[1], Yan Qiu[1], Shiying Li[1], Jiaoyue Hu[1], Wei Li[1], Jianfeng Wu[4], Haiwei Xu[5,6], Steven J. Fliesler[7,8], Yi Liao[1]✉ and Zuguo Liu[1,2,3]✉

Mammalian Müller glia (MG) possess limited regenerative capacities. However, the intrinsic capacity of mammalian MG to transdifferentiate to generate mature neurons without transgenic manipulations remains speculative. Here we show that MAP4K4, MAP4K6 and MAP4K7, which are conserved Misshapen subfamily of ste20 kinases homologs, repress YAP activity in mammalian MG and therefore restrict their ability to be reprogrammed. However, by treating with a small molecule inhibitor of MAP4K4/6/7, mouse MG regain their ability to proliferate and enter into a retinal progenitor cell (RPC)-like state after NMDA-induced retinal damage; such plasticity was lost in YAP knockout MG. Moreover, spontaneous trans-differentiation of MG into retinal neurons expressing both amacrine and retinal ganglion cell (RGC) markers occurs after inhibitor withdrawal. Taken together, these findings suggest that MAP4Ks block the reprogramming capacity of MG in a YAP-dependent manner in adult mammals, which provides a novel avenue for the pharmaceutical induction of retinal regeneration in vivo.

npj Regenerative Medicine (2023)8:36 ; https://doi.org/10.1038/s41536-023-00310-6

INTRODUCTION

Loss of photoreceptors and retinal ganglion cells (RGCs) results in vision loss in prominent retinal diseases, such as age-related macular degeneration, diabetic retinopathy, and glaucoma. Neither photoreceptors nor RGCs possess endogenous regenerative capabilities, hence, presenting a major impediment to developing cures for these blinding diseases. Regenerative medicine approaches have been tried to solve this problem, e.g., by transplanting stem/progenitor cells or their derived cells into the retina, but the outcomes have been variable and, in general, have not been effective[1]. Besides, some cold-blooded vertebrate species, such as fish and amphibians, are able to regenerate retinal neurons from endogenous MG[2–4], which has inspired new ideas about how to repair damage to retinal neurons caused by various genetic, environmental, or traumatic insults.

Although unable to regenerate retinal neurons, mammalian MG retain some stem/progenitor cell characteristics in vitro[5] and in vivo[6]. Even more attractive, early studies demonstrated that mouse MG express the cell cycle gene CyclinD3[7] and upregulate the retinal progenitor cell (RPC) marker Pax6[8] in response to retinal injury, which closely mimics the activation pattern observed in fish MG. Later, one landmark study proved the regenerative potential of mammalian MG by intravitreal injection of growth factors, which converts MG into amacrine cells[9]. Recently, both gain-of-function and loss-of-function methods have successfully converted mouse MG into retinal neurons, including photoreceptors[10], bipolar/amacrine cells[11–13], as well as RGCs[14–16] in various mouse models. Despite these achievements, however, all these studies involved manipulation of gene expression using transgenic strategies, which has largely limited their clinical translational potential. In addition, since exogenous transcription factors were introduced, it remains an open question whether mammalian MG retain the ability to transdifferentiate into photoreceptors and RGCs.

Without growth factors or exogenous genes, mammalian MG only temporarily express cell cycle genes and the Pax6 gene in response to retinal damage, so reactive gliosis ensues within a day or so. Therefore, it is reasonable to suspect that endogenous blocking mechanisms exist that can repress regenerative capabilities of MG. Recently, cross-species sequencing has revealed that the Hippo pathway plays a pivotal role in restoring reactive MG to a quiescent state after retinal injury in mice[13]. Specifically, conditional deletion of Yes associated protein 1(YAP1, also known as YAP, a transcriptional regulator of cellular proliferation and apoptosis)[17,18] in MG, a key downstream effector protein of the Hippo pathway, was shown to prevent the upregulation of cell-cycle entry genes in reactive MG in both NMDA- and MNU-damaged retina[19,20]. Moreover, over-activation of YAP has been shown to be able to drive MG into a progenitor-like state after retinal injury in mice[20]. All these lines of evidence indicate that the Hippo pathway could be a druggable target for retinal neuron regeneration in mammals.

The Hippo signaling pathway was initially identified in model organism *Drosophila*, which plays fundamental roles in organ size regulation, development, tissue regeneration and tumorigenesis[17]. In the canonical Hippo pathway, Ste-20 family kinase Mst1/2 phosphorylates and activates NDR family kinase LATS1/2 and cofactor MOB1/2, which subsequently phosphorylates and sequesters YAP/TAZ in the cytoplasm. However, one intriguing

[1]Department of Ophthalmology, Xiang'an Hospital of Xiamen University; Fujian Provincial Key Laboratory of Ophthalmology and Visual Science; Fujian Engineering and Research Center of Eye Regenerative Medicine; Eye Institute of Xiamen University; School of Medicine, Xiamen University, Xiamen, Fujian 361005, China. [2]Xiamen University Affiliated Xiamen Eye Center, School of Medicine, Xiamen University, Xiamen, China. [3]Department of Ophthalmology, the First Affiliated Hospital of University of South China, Hengyang, Hunan 421001, China. [4]Laboratory animal research center, Xiamen University, Xiamen, Fujian 361102, China. [5]Southwest Hospital/Southwest Eye Hospital, Third Military Medical University (Army Medical University), Chongqing, China. [6]Key Lab of Visual Damage and Regeneration & Restoration of Chongqing, Chongqing 400038, China. [7]Departments of Ophthalmology and Biochemistry and Neuroscience Graduate School, Jacobs School of Medicine and Biomedical Sciences, SUNY- University at Buffalo, Buffalo, NY, USA. [8]Research Service, VA Western New York Healthcare System, Buffalo, NY, USA. ✉email: liaoyilori@xmu.edu.cn; zuguoliu@xmu.edu.cn

finding is that LATS1/2 can still be phosphorylated in both Mst1/2-null mouse embryonic fibroblasts (MEFs) and hepatocellular carcinoma cells (HCCs)[21]. As a result, multiple studies have demonstrated that mitogen-activated protein kinase kinase kinase kinase (MAP4K) family members, particularly HPK/GCK-like kinase (HGK/MAP4K4), misshapen-like kinase 1 (MINK1/MAP4K6), and Nck-interacting kinase (TNIK/MAP4K7) can work in parallel with Mst1/2 to phosphorylate LATS1/2 and regulate YAP/TAZ activities[22,23]. However, the physiological and pathological relevance of MAP4Ks-regulated YAP phosphorylation are yet to be fully elucidated.

Thus, we hypothesized that MAP4Ks might block mammalian MG regenerative capabilities by suppressing the YAP/TAZ activities. Accordingly, by using a highly selective small-molecule compound, DMX-5804, which simultaneously inhibits MAP4K4/6/7 to inhibit cell death and augment mitochondrial function and calcium cycling[24], we showed that MAP4K4/6/7 converge to inhibit YAP activity in human and mouse MG. Notably, inhibition of MAP4K4/6/7 kinase activities in the early stage of retinal injury promoted MG proliferation and transformation into an RPC-like state by activating YAP. Even more exciting, long-term tracing experiments demonstrated the intrinsic ability of mammalian MG to regenerate amacrine and RGC-like neurons after NMDA-induced inner retinal neuron injury, which opens a new window for future advances in retinal regenerative medicine.

RESULTS

MAP4K4/6/7 are expressed in mammalian MG

First, the protein expression levels of MAP4K4/6/7 isoforms were measured in adult murine retinas (~ 8 wk old) injured by intravitreal injection of N-methyl-D-aspartate (NMDA); age-matched mice were injected with same volume of vehicle (PBS) alone to serve as controls. Compared with PBS controls, we observed a progressive increase of all three kinases in protein levels (Fig. 1a–d) beginning from 12 h after NMDA injection, and their expression levels were maximal by 24 h after NMDA injection. Elevated expression levels of these three kinases persisted in the neuroretina for the next 3 days (Fig. 1a–d). MAP4Ks directly phosphorylate the hydrophobic motif of LATS kinases, and LATS1/2 subsequently phosphorylate YAP[22]. As surrogates to represent MAP4K4/6/7 activities, we next examined the phosphorylation of LATS1 and YAP (Fig. 1a, e, f) in the neuroretina by Western blot analysis after NMDA treatment. A similar elevated pattern was observed for MAP4K4/6/7 expression levels, LATS1 phosphorylation and YAP phosphorylation (Fig. 1a–f), which is a harbinger of a possible relationship between MAP4Ks and YAP activity.

Next, immunostaining was performed to determine the localization of MAP4K4/6/7 isoforms in the adult murine retina. As revealed by Immunofluorescence, MAP4K4/6/7 isoforms were present in all of the histological layers and all of their cell types in the neural retina (Fig. 1g–j). Co-localization analysis showed that MAP4K4/6/7 were expressed in the same cells as YAP was (Fig. 1k–n), a critical transcription cofactor downstream of the Hippo pathway. Previously, YAP was reported to be specifically expressed in murine MG[25]. Therefore, these results confirmed that MAP4K4/6/7 were co-expressed with YAP in mature mouse MG, and indicated a possible regulatory role of MAP4Ks for YAP activity.

MAP4K4/6/7 Work Redundantly to Regulate YAP Phosphorylation in Mammalian MG

Considering the co-localization and similar expression trends of MAP4K4/6/7 and YAP phosphorylation in NMDA-injured murine retina, we next tried to determine whether MAP4Ks regulated YAP activity in MG. MAP4K4/6/7 were expressed in the human MG cell line MIO-M1, which expresses MG markers glutamine synthetase (GS) and glial fibrillary acidic protein (GFAP) (Supplementary Fig. 1a). Among MAP4Ks, MAP4K4, MAP4K6 and MAP4K7 belong to the same GCK kinase family, and they share high sequence and structural similarities[26]. MAP4K4 was shown to have the strongest ability to regulate YAP activity, while MAP4K6/7 work in concert with MAP4K4 in HEK293A cells[22]. When we used siRNA to selectively knock down MAP4K4 alone by ~90%, there was no effect on YAP phosphorylation levels (Supplementary Fig. 1b–d). However, when we simultaneously knocked down MAP4K4, MAP4K6 and MAP4K7 in MG, we observed a ~ 50% decrease of YAP phosphorylation (Supplementary Fig. 1e, f [$p = 0.0004$]) as well as an increase of YAP nuclear translocation (Supplementary Fig. 1g, h [$p = 0.0015$], i [$p = 0.0019$]). Taken together, these results suggested that MAP4K4, MAP4K6 and MAP4K7 work redundantly to regulate YAP phosphorylation in MG.

Cross-species analysis[13] and transgenic studies[19,20] all demonstrated that YAP plays critical roles in regulating MG proliferation after induced retinal damage. We next assessed the effect of MAP4K4/6/7 siRNA mix on cell proliferation in MIO-M1 cells. Using ki67 as an indicator for proliferative cells, we found that knockdown of MAP4K4/6/7 increased the proliferation profile of MG by about 10% (Supplementary Fig. 2a, b [$p = 0.0219$]). Subsequently, we purified and cultured primary MG from Glast-CreERT2^{+}/tg;ROSA26R-tdTomato + /tg mice, which specifically label MG with tdTomato fluorescent proteins[20]. Even more interestingly, we observed neurite outgrowth and expression of the RGC/amacrine cells marker HuC/D in cells where MAP4K4/6/7 were knocked down (Supplementary Fig. 2c). These results suggested that MAP4K4/6/7 might be druggable targets to modulate MG regenerative abilities in vivo.

DMX-5804 Suppresses MAP4K4/6/7-mediated YAP Phosphorylation in Mammalian MG

Next, we hypothesized that pharmacological suppression of MAP4K4/6/7 could alleviate YAP phosphorylation and promote the nuclear localization of YAP in MG. Accordingly, a small-molecule inhibitor DMX-5804, which exhibits high potency and selectivity towards MAP4K4/6/7[24], was utilized to suppress YAP phosphorylation in MG in vitro and in vivo. Indeed, the application of DMX-5804 in culture media decreased YAP phosphorylation in MIO-M1 cells in a dose- and time-dependent manner (Supplementary Fig. 3a–d). Also, YAP nuclear translocation was observed when MIO-M1 cells were treated with DMX-5804 (Supplementary Fig. 3e–g).

Next, we assessed the effect of DMX-5804 in vivo. An escalating dose-response assay showed that DMX-5804 blocked YAP phosphorylation in the neuroretina at 6 h after intraperitoneal (*i.p.*) injection (dose range: 0.5 mg/kg to ~10 mg/kg) in comparison with the solvent control (Supplementary Fig. 4a–d). In addition, a single *i.p.* injection of 2 mg/kg DMX-5804 could suppress YAP phosphorylation by ~40% for more than 6 h in the intact adult murine retina (Supplementary Fig. 4e, f). Immunofluorescence staining further verified that DMX-5804 treatment promoted YAP nuclear translocation in MG, which was assessed by the co-localization with MG nuclear markers SOX9 (SOX9 + MG) (Supplementary Fig. 4g–i). Importantly, these results suggested that the lipid-soluble small molecule DMX-5804 possesses the ability to cross the blood-retinal barrier to regulate YAP activities in MG when drug is administrated systemically (i.e., by *i.p.* injection).

To assess the effect of DMX-5804 in the NMDA-injured retina, we developed a protocol for continuous *i.p.* injection (4 injections per day, from 6 h post-NMDA injection until 5 days post-NMDA injection) in a mouse model with NMDA-induced retinal degeneration (Fig. 2a). A progressive increase in both LATS1 and YAP phosphorylation was observed in the NMDA-damaged neuroretina, and phosphorylation levels of both proteins were reduced after DMX-5804 treatment (Fig. 2b, c

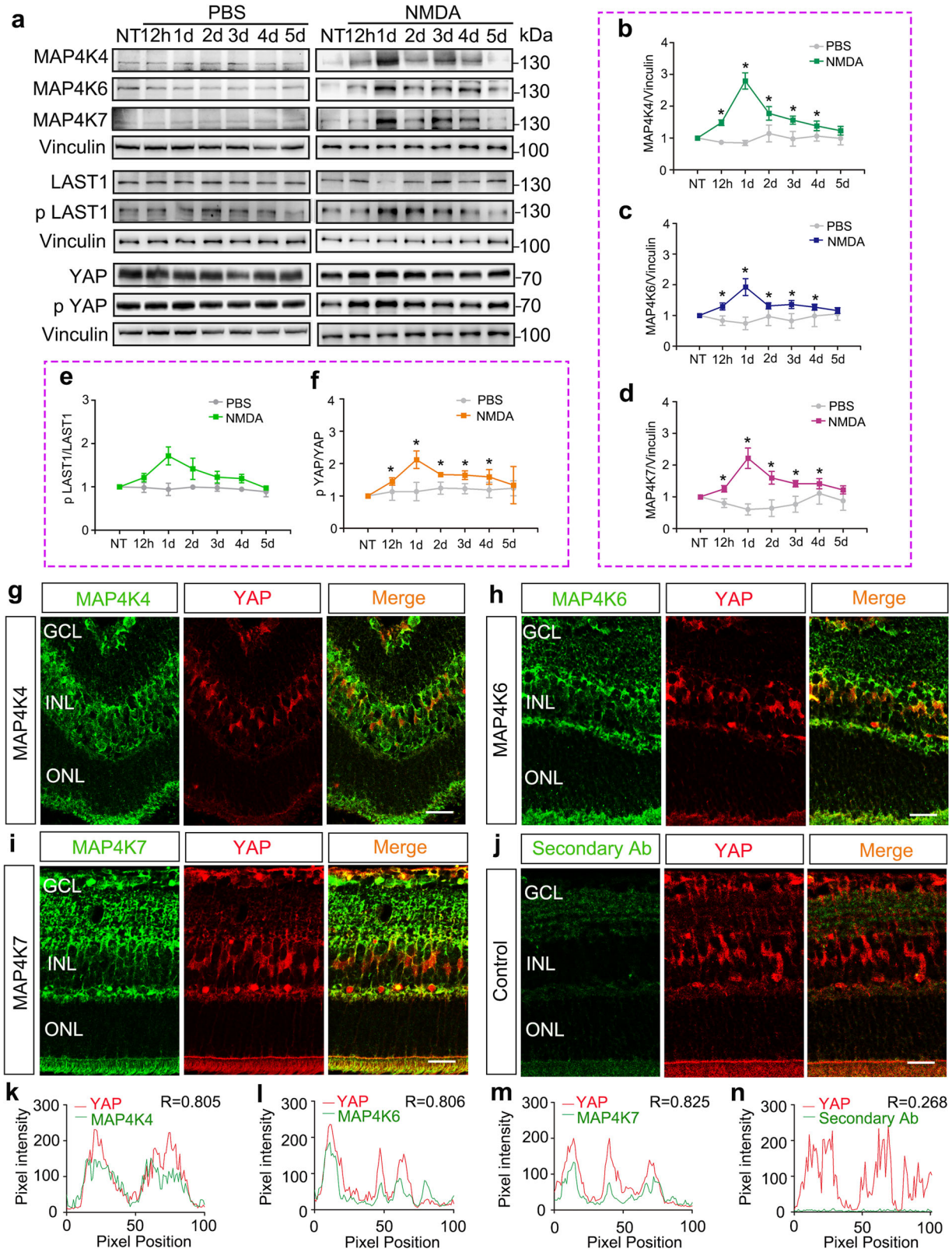

Fig. 1 MAP4K4/6/7 expression and YAP phosphorylation after retinal injury in MG. a Western blots analysis of MAP4K4/6/7, p LATS1/LATS1 and p YAP/YAP in the NMDA-injured retina. **b**–**f** Quantification of MAP4K4(**b**)/6(**c**)/7(**d**), p LATS1/LATS1(**e**) and p YAP/YAP(**f**) protein expression in (**a**). **g**–**j** Immunofluorescence staining of MAP4K4 (**g**), MAP4K6 (**h**), MAP4K7 (**i**) together with YAP in the sections of murine retina. MG were specifically stained with YAP. The section stained with secondary antibody (**j**) was served as negative control. **k**–**n** Co-localization analysis of MAP4K4/6/7/negative control and YAP in (**g**–**i**). Scale bars, 20 μm (**g**–**j**). For Western blots, levels were given as a.u. ± SEM in comparison with PBS or no-treatment (NT) controls (4 samples per pool; $n = 3$ independent pools of samples per group; Student's t-test). For co-localization analysis, evaluation results were given as Pearson correlation coefficient. $^{*}p \le 0.05$, $^{**}p \le 0.01$, $^{***}p \le 0.001$.

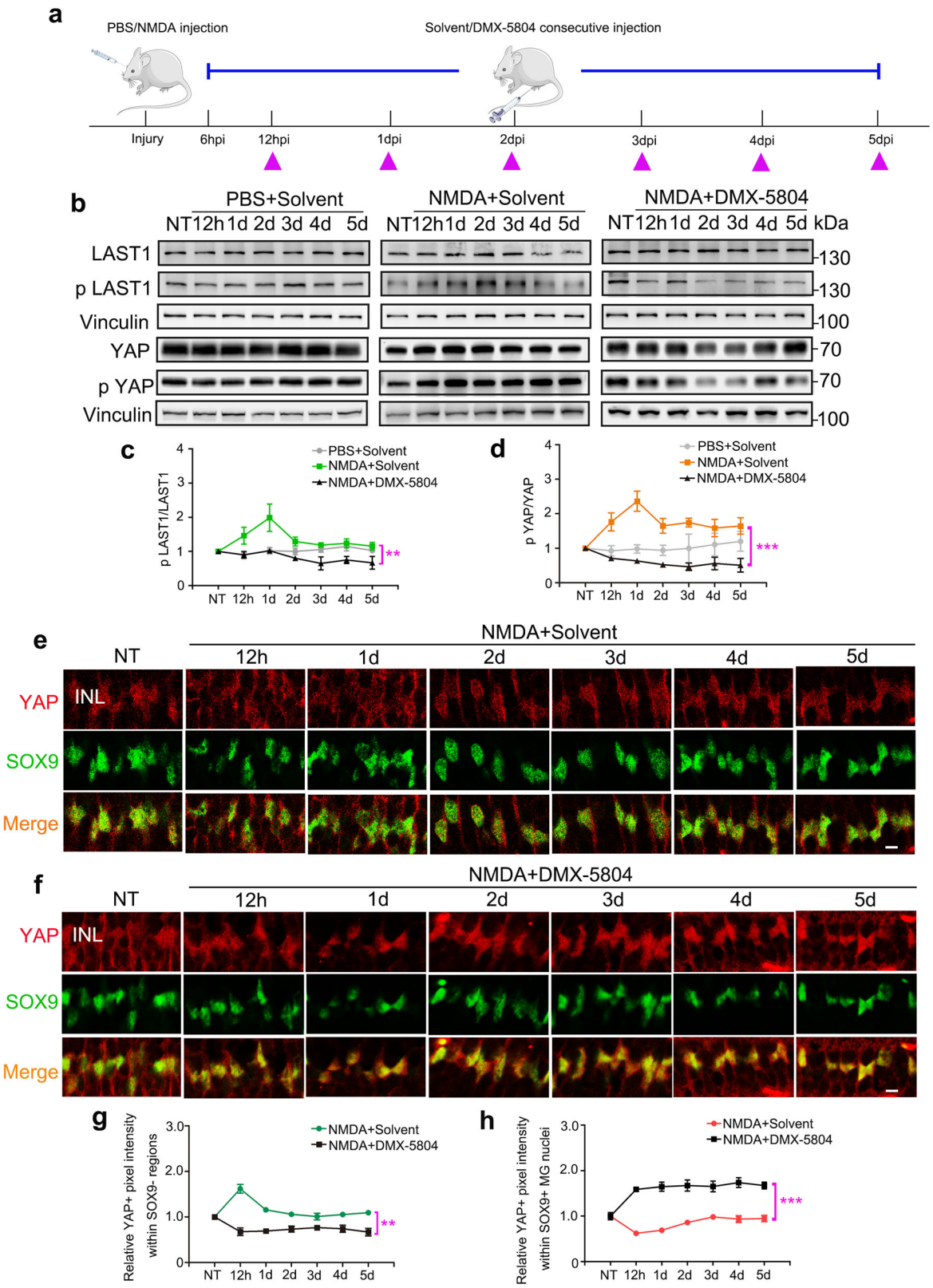

[$p = 0.0002$], d [$p = 0.0001$]). Moreover, more YAP was translocated into the nucleus of MG in DMX-5804 treated mice (Fig. 2e–h). Taken together, these data indicate that targeting MAP4K4/6/7 activates YAP and promotes YAP nuclear translocation in reactive MG.

DMX-5804 promotes MG proliferation in the NMDA-injured retina

In previous studies, mice carrying a constitutively active YAP5SA transgene possess more EdU$^+$ MG and more cells reside in a progenitor-like state after retinal damage[20]. Thus, we assumed

Fig. 2 The translocation of YAP into the nuclei of MG after NMDA/DMX-5804 treatment. a Timeline diagram of the experimental procedure used in (**b-i**). Wildtype mice were intravitreally injected with NMDA. Solvent control or DMX-5804 was injected every 6 h intraperitoneally from 6 h post-NMDA injection (hpi) until 5 days post-NMDA injection (dpi). The purple triangles represent the time points of the sampling. **b** Western blot analysis of p LATS1/LATS1 and p YAP/YAP in the murine neuroretina treated with PBS/solvent, NMDA/solvent and NMDA/DMX-5804. **c**, **d** Quantification of p LATS1/LATS1 and p YAP/YAP (normalized to vinculin) protein expression in **b**. **e** Immunofluorescence staining of YAP (*red*; YAP +) and SOX9 (*green*; SOX9 +) at indicated time points in the NMDA-injured murine retina. **f** Immunofluorescence staining of YAP (*red*; YAP +) and SOX9 (*green*; SOX9 +) at indicated time points in the NMDA-injured murine retina treated with DMX-5804. **g** Quantification of relative YAP+ pixel intensity in SOX9- MG regions in (**e**, **f**). **h** Quantification of relative YAP+ pixel intensity in SOX9 + MG nuclei in (**e**, **f**). For western blots, levels were given as a.u. ± SEM in comparison with solvent or no-treatment (NT) (4 samples per pool; $n = 3$ independent pools of samples per group; one-way ANOVA test). Scale bars, 20 μm (**e**, **f**). For pixel intensity measurements, levels were given as mean ± SEM ($n = 6$ mice per group; one-way ANOVA test). The one-way ANOVA test was performed between the NMDA+Solvent group and the NMDA + DMX-5804 group. *$p \le 0.05$, **$p \le 0.01$, ***$p \le 0.001$.

that suppression of MAP4K4/6/7 pharmacologically may promote MG proliferation and dedifferentiation into a progenitor-like state. To test this hypothesis, we assessed MG proliferation using EdU labeling when DMX-5804 was injected into NMDA-treated mice following a protocol we depicted in Fig. 3a. Consistent with previous studies[8,27], we failed to detect EdU$^+$ MG, which were marked by nuclear staining of Sox9, in control (non-treated, NT), NMDA-treated or NMDA/solvent control groups (Fig. 3b). In contrast, DMX-5804 treatment promoted a number of reactive MG to proliferate on the 3rd day after NMDA-induced damage, as shown by EdU$^+$ labeling in SOX9$^+$ cells (Fig. 3b). Moreover, we observed double-positive (EdU$^+$/GFAP$^+$) cells after DMX-5804 treatment in the injured retina, suggesting that MG in the adult murine retina might undergo a reprogramming event accompanying with a gliotic response (characterized by MG hypertrophy and increased GFAP expression) similar to zebrafish (Fig. 3c). Close examination revealed that these proliferating cells exhibited similar morphologies (Fig. 3c) as clonally expanding zebrafish progenitor-like cells derived from MG[28,29].

To evaluate DMX-5804-promoted MG proliferation in detail, mice were treated following the protocol described in Fig. 2a. Subsequently, EdU was *i.p.* injected 24 h before the collection of retinal samples (Fig. 3d). It is worthy to notice that a few EdU$^+$/SOX9$^+$ MG began to appear at 2 dpi, and this population reached the maximum number at 3 dpi (Fig. 3e–h). In addition, we used another mouse strain (Glast-CreERT2$^+$/tg;ROSA26R-tdTomato + /tg mice) to specifically label MG[20] and examined the effect of DMX-5804 on MG proliferation. We immunostained the sections with antibodies to two other cell proliferation markers (ki67 and PCNA) at 3 dpi, and we found nearly 100% co-localization of ki67/PCNA and EdU in tdTomamto+ cells (Supplementary Fig. 5). However, the number of EdU+tdTomato+ cells was dramatically decreased at 4 dpi and 5 dpi despite continuous DMX-5804 application (Fig. 3e–h), and they were merely observed after 6 days post-injury (data not shown).

DMX-5804 induces the dedifferentiation of MG into a progenitor-like state in the NMDA-injured retina

Pax6 is highly expressed by retinal progenitors in the developing retina and inner retinal neurons (i.e., amacrine cells and RGCs)[30]. The re-emergence of Pax6 expression is a well-documented step during the process of de-differentiation of MG after retinal damage in both fish and chicken in vivo[9,31,32] as well as in adult rats in vitro[33]. Moreover, unbiased single-cell mRNA sequencing (scRNA-seq) transcriptome analysis has suggested YAP5SA + MG-derived cells could express Pax6[20]. Thus, the expression of Pax6 in MG after DMX-5804 treatment was examined by immunofluorescent staining of retinal sections from NMDA-damaged eyes (Fig. 4a). The staining results demonstrated that the YAP$^+$/Pax6$^+$ cell population expanded in MG with a similar Pax6 fluorescence intensity as the amacrine-rich layer after NMDA/DMX-5804 injections, while much a lower expression level of Pax6 was detected in MG in NMDA/solvent group (Fig. 4b, c).

DMX-5804 reprograms MG into retinal neurons in the NMDA-injured retina

Next, we traced the fate of Pax6$^+$ MG in the retinas of Glast-CreERT2$^+$/tg;ROSA26R-tdTomato + /tg mice. We observed apical translocation of Pax6$^+$ MG nuclei to the inner nuclear layer (INL) and outer nuclear layer (ONL) at day 3 after NMDA-induced damage was initiated and DMX-5804 continuous treatment (Fig. 4d, e), which we suspect is a similar process as that termed "interkinetic nuclear migration" (INM) observed during MG-mediated regeneration in zebrafish[34]. To check if these ONL translocated MG might generate photoreceptors, we immunostained the retinal sections for rod and cone photoreceptor markers. However, we could not detect any MG-derived cells expressing photoreceptor specific markers at 3 dpi and no tdTomato+ cell was observed in ONL by 9 dpi (Supplementary Fig. 6a, d, e). Moreover, we discovered a substantial cohort of tdTomato-positive cells could be labelled by both EdU and Pax6 (Edu$^+$/Pax6$^+$), suggesting the appearance of proliferating RPC-like cells (Fig. 4e, f). More interestingly, we found some *triply* labeled (EdU + /NeuN + /tdTomato +) cells after 3 days of NMDA/DMX-5804 injections (Fig. 4e, g). Also, we found these tdTomato+ cells began to express HuC/D (a marker for both RGCs and amacrine cells) at 3 dpi (Supplementary Fig. 6a–c), and expressed RGCs marker MAP2 and RGCs/amacrine cells marker Calretinin 9 days after NMDA/DMX-5804 treatment (Supplementary Fig. 6e). Therefore, these results suggested that the conversion of proliferating MG into neurons occurred at an early stage of NMDA/DMX-5804 treatment.

In order to facilitate the observation of cell reprograming process after NMDA or NMDA/DMX-5804 treatment, neuroretinas were flattened and stained to monitor a variety of reprogrammed cells in the whole retina simultaneously (Supplementary Fig. 7a). Consistently, we only discovered reprogrammed tdTomato$^+$ MG in the NMDA/DMX-5804 group, which were absent in the NMDA group. In addition, three types of reprogrammed tdTomato$^+$ MG were observed, including EdU$^+$/NeuN$^-$/tdTomato$^+$ MG (*white box*), EdU$^+$/NeuN$^+$/tdTomato$^+$ MG (*yellow box*) and EdU$^-$/NeuN$^+$/tdTomato$^+$ MG (*purple box*) (Supplementary Fig. 7b). We suspected these cells could represent three different reprogramming states, respectively: 1) MG that entered the cell cycle but without trans-differentiation; 2) MG-derived neurons after cells complete a cell cycle; and 3) MG-derived neurons without entering a cell cycle. Thus, notably, our results indicated that MG have the ability to trans-differentiate into neurons in both a cell cycle-*dependent* and a cell cycle-*independent* manner after NMDA/DMX-5804 treatment. As we observed ~ 6-fold more double-labeled (EdU-/NeuN + /tdTomato+ cells) than triply-labeled (EdU + /NeuN + /tdTomato +) cells (Fig. 4e, g [$p < 0.0001$]), we suspected that most proliferative MG after DMX-5804 treatment were used to sustain the MG population.

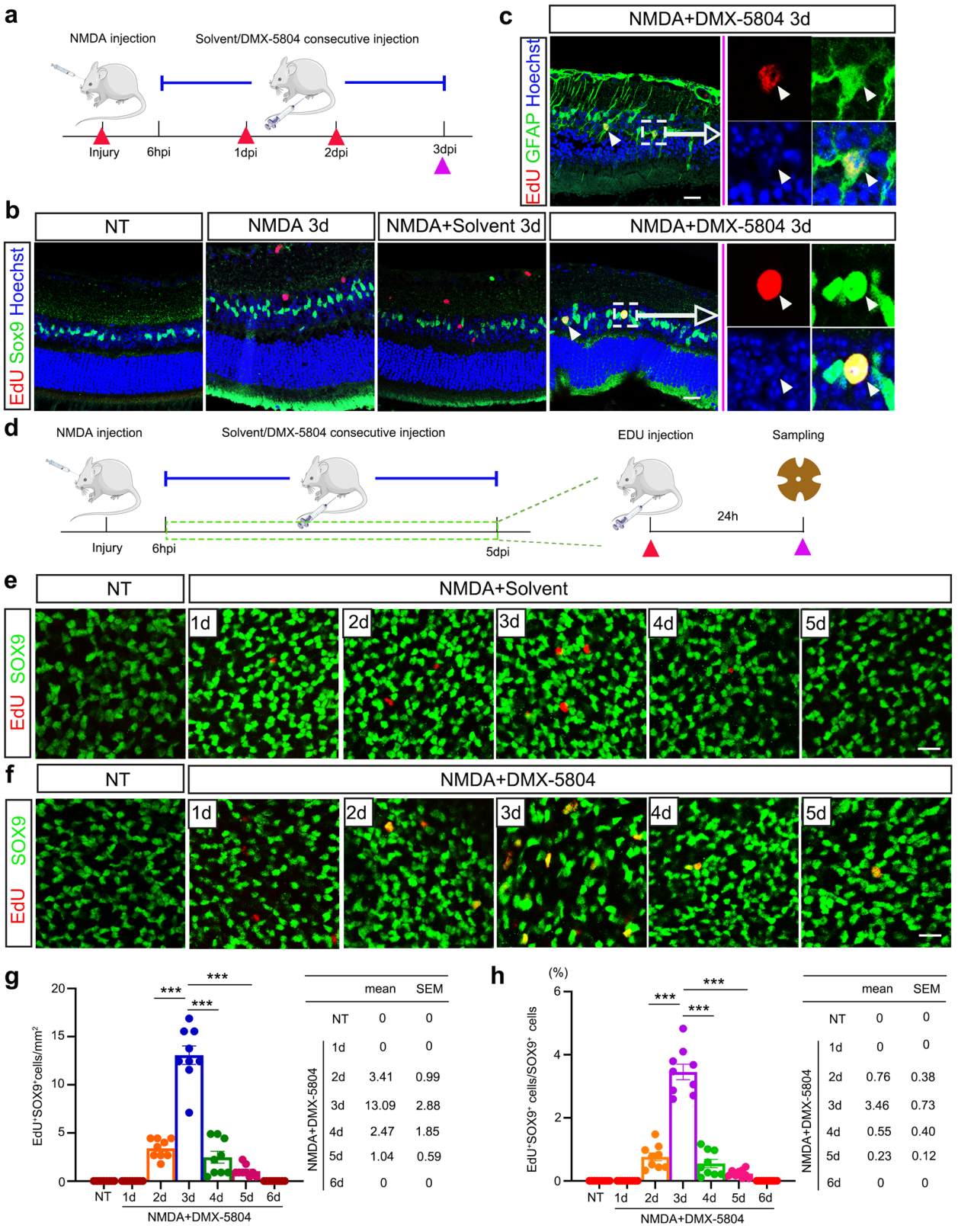

DMX-5804 promotes MG plasticity in a YAP-dependent manner in the NMDA-injured retina

To test if the effect of DMX-5804 is YAP dependent, we delivered Cre tagged with enhanced green fluorescence protein (EGFP) into adult Yap$^{flox/flox}$ mouse retina under the control of GFAP promoter by intravitreal injection of adeno-associated viruses (AAVs, type 2/9) (Fig. 5a, b). Loss of YAP staining in SOX9^{+}/EGFP^{+} MG was shown in retinal sections, suggesting that the Yap gene in EGFP^{+} MG was successfully removed by Cre recombinase (Fig. 5c). In these AAV-treated mice (Fig. 5d), we found a decrease of EdU^{+} cells as well as

Fig. 3 Proliferation of MG in the NMDA-injured murine retina with or without DMX-5804 treatment. a Timeline diagram of the experimental procedures used in **b** and **c**. Wildtype mice were intravitreally injected with NMDA. Solvent control or DMX-5804 was injected following the same protocol depicted in Fig. 2a. EdU was injected intraperitoneally every 24 h after NMDA injury till mice scarification. The *red* triangles represent the time points of the EdU injection and the *purple* triangles represent the time points of the sampling. **b** EdU labeling (*red*) and SOX9 immunofluorescence (*green*) on retinal sections after NMDA, NMDA/solvent or NMDA/DMX-5804 treatment. **c** EdU labeling (*red*) and SOX9 immunofluorescence (*green*) on retinal sections after NMDA/DMX-5804 treatment. **d** Timeline diagram of the experimental procedures used in (**e**–**h**). Wildtype mice were intravitreally injected with NMDA. Solvent or DMX-5804 was injected using the same method depicted in Fig. 2a. A single dose of EdU was injected intraperitoneally 24 h before mice were sacrificed. **e** EdU labeling (*red*) and SOX9 immunofluorescence (*green*) on whole flat-mounted retinas at indicated time points after NMDA/solvent treatment. **f** EdU labeling (*red*) and SOX9 immunofluorescence (*green*) on whole flat-mounted retinas at indicated time points after NMDA/DMX-5804 treatment. **g** Quantification of the number of cells positive for both EdU labeling (EdU +; *red*) and SOX9 immunofluorescence (SOX9 +; *green*) per mm^2 in (**f**). **h** Quantification of the percentage of cells positive for both EdU labeling (EdU +; *red*) and SOX9 immunofluorescence (SOX9 +; *green*) in (**f**). Scale bars, 20 μm (**b**, **c**) or 15 μm (**e**, **f**). For quantification of EdU+ SOX9+ cells, levels were given as mean ± SEM ($n = 9$ mice per group; Student's *t*-test). *$p \le 0.05$, **$p \le 0.01$, ***$p \le 0.001$.

$EdU^+/SOX9^+$ cells in $Yap^{flox/flox}$ mice *vs*. in wild type mice after NMDA and DMX-5804 treatment (Fig. 5e–h).

When translocated into the nucleus, YAP binds to the transcription factors TEAD1-4 to promote their activity[35]. To further determine whether YAP functioned downstream of MAP4K4/6/7 to mediate MG proliferation, we used verteporfin, an inhibitor that prevents YAP-TEAD complex formation, together with DMX-5804 to treat mice for 5 days after NMDA-induced retinal damage; EdU was injected *i.p*. and retinal samples were collected (Supplementary Fig. 8a). Compared with the group treated with DMX-5804 only, we observed a decrease in the number of $EdU^+/SOX9^+$ MG in the NMDA-damaged retina in the mice when DMX-5804 and verteporfin were injected together (Supplementary Fig. 8b–d).

In addition, the emergence of Pax6+ progenitors from MG and their differentiation were examined in AAV-treated $Yap^{flox/flox}$ mice. We found a nearly 50% decrease of Pax6+ cells (Fig. 5i, j [$p < 0.001$]) and more than a 4-fold reduction of NeuN+ cells (Fig. 5i, k [$p < 0.001$]) in EGFP+ cells where the expression of Yap was almost fully diminished. Taken together, these results confirmed that YAP is the downstream target of DMX-5804 to promote MG proliferation and trans-differentiation after retinal damage.

DMX-5804 Induces the Expression of Proneural Transcription Factors in MG in the NMDA-Injured Retina

During development, retinal progenitors express several key proneural transcription factors, including Ascl1, Atoh1/7, Pou4f2 and Isl1, which are critical to maintain progenitor pool and determine retinal neuron fate[16,36]. Among them, Ascl1 regulates retinal progenitor pool and induces neuronal fate, while Atoh1/7 has been regarded as a fate determinant of RGC lineage. In addition, Pou4f2 and Isl1 are known to regulate RGC specification and differentiation[12,16,36]. All of these lineage-specific transcription factors have been reported to affect MG neurogenic capacities previously[16]. To test whether MG after NMDA/DMX-5804 treatment acquired the ability to transdifferentiate into neurons, we used droplet digital PCR to determine the expression level of several key transcription factors in isolated MG. Adult Glast-CreERT2 + /tg; ROSA26R-tdTomato + /tg mice were induced with tamoxifen followed by NMDA/DMX-5804 injection. Subsequently, tdTomato+ cells were isolated by fluorescence-activated cell sorting (FACS) at different time points (Supplementary Fig. 9a). We detected the increased expression of *Ascl1* from 3 dpi to 10 dpi, and *Atoh7* from 10 dpi to 15 dpi in MG after NMDA/DMX-5804 induction (Supplementary Fig. 9b–d). However, we failed to detect *Atoh1*, *Pou4f2* and *Isl1* expression from 0 to 20 dpi (Supplementary Fig. 9b), indicating NMDA/DMX-5804 induced-MG derived neuron-like cells may not reach the maturity. Nonetheless, our data suggested that MG acquired the potential to convert to the RGC lineage after NMDA/DMX-5804 treatment.

Long-term effect of DMX-5804 treatment on retinal regeneration

To elucidate how efficiently reprogrammed MG could turn into neurons and further determine their eventual fate, we traced MG for 30 days after NMDA/DMX-5804 treatment using Glast-$CreERT2^+$/tg;$ROSA26R\text{-}tdTomato^+$/tg mice (Fig. 6a). Although $NeuN^+/tdTomato^+$ cells were absent in the normal, NMDA-damaged or NMDA/solvent treated retinas (Supplementary Fig. 10a, b), they appeared in the GCL and INL of retinas after NMDA/DMX-5804 treatment (Supplementary Fig. 10c–e). We found only a couple of $tdTomato^+$ cells co-expressed GAD67 (Fig. 6b, c), a marker of amacrine cells[30]. In addition, we surprisingly found several $tdTomato^+$ cells could be labeled by RNA binding protein with multiple splicing (RBPMS) or βIII-tubulin, two well-acknowledged markers of RGCs[37,38], indicating DMX-5804 treated MG might transdifferentiate into RGC-like cells (Fig. 6b, c). However, $tdTomato^+/GAD67^+$, $tdTomato^+/RBPMS^+$ and $tdTomato^+/\beta III\text{-}tubulin^+$ cells were very rare (Fig. 6d, e). Therefore, we set up another paradigm to further confirm the existence of MG-derived RGC-like cells at 30 dpi after NMDA/DMX-5804 treatment. A curtate GFAP promoter was used to increase the label specificity of MG[10,39] and MG-specific AAV variants were used (Supplementary Fig. 11a). After intravitreal injection of AAV2/8-short GFAP-EGFP for 3 wks, we detected the strongest green fluorescence signal in the mouse retina (Supplementary Fig. 11b, c). When retinal neurons were stained with NeuN antibodies and MG were stained with Sox9 antibodies, $EGFP^+$ signal was only detected in $SOX9^+$ cells, further confirming that MG were labeled specifically and their identities were not affected by the injection and treatment with AAVs (Supplementary Fig. 11d). NMDA/DMX-5804 treatment was carried out at the 3rd week after AAVs injection when EGFP signals reached their highest level (*data not shown*). Subsequently, the retinal samples were collected on 30 dpi (Supplementary Fig. 12a). Immunofluorescent staining of retinal flat mounts or transverse cryosections showed the presence of $NeuN^+/EGFP^+$ cells in the GCL and INL of retinas after NMDA/DMX-5804 treatment, while they were absent after NMDA/solvent treatment (Supplementary Fig. 12b, d, e). Moreover, we also found a small quantity of $GAD67^+/EGFP^+$ cells located in the INL (Supplementary Fig. 12c). Very occasionally, $RBPMS^+/EGFP^+$ cells were observed in the GCL (Supplementary Fig. 12c). Thus, despite a relatively high conversion efficiency from MG into neurons ($NeuN^+$ MG-derived cells), only a very small fraction of converted cells could further differentiate into mature neuronal cells expressing the markers of amacrine cells or RGCs.

To test the translational value of DMX-5804, we performed electroretinography (ERG) to examine photopic negative responses (PhNRs), which measures the function of RGCs across the entire retina[40,41], in NMDA/DMX-5804-treated mice. Surprisingly and notably, we detected an ~2-fold improvement in the

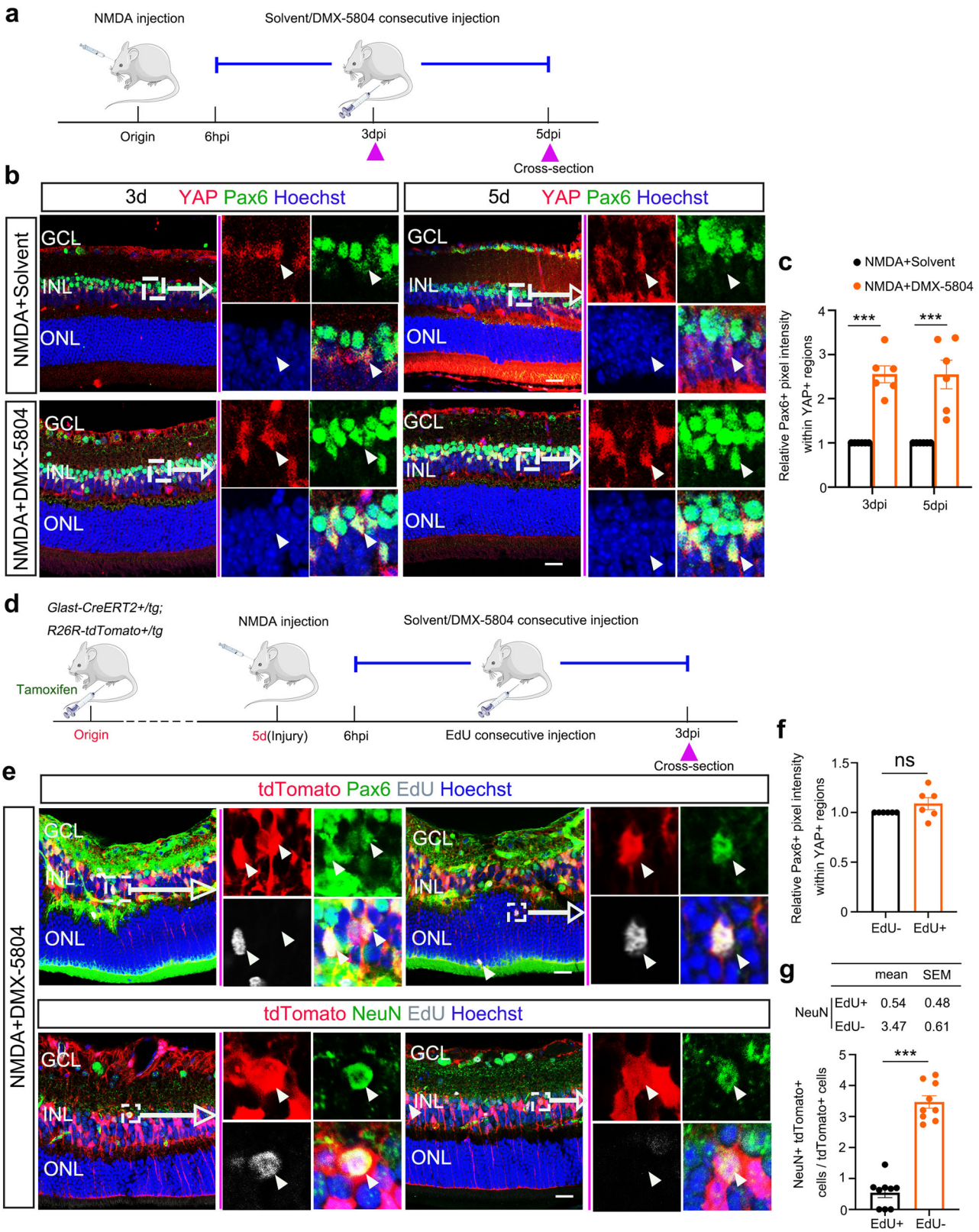

magnitude of the PhNR response in mice that received NMDA/DMX-5804, in comparison with mice that only received NMDA treatment alone (Fig. 6f). Considering that DMX-5804 was administrated systematically, we also collected major organs (including heart, brain, liver, intestine, spleen, lung and kidney) from mice to evaluate (by standard histopathology methods) the safety of DMX-5804. However, we could not detect any appreciable alterations in cellular morphology, cell proliferation or cell death in major tissues after DMX-5804 treatment (Supplementary Fig. 13).

Fig. 4 MGs enter into retinal progenitor cell-like state and transdifferentiate into neurons after NMDA/DMX-5804 treatment. a Timeline diagram of the experimental procedure used in (**b**). The mice were treated following the experimental procedures depicted in Fig. 2a. The *purple* triangles represent the time points of the sampling. **b** YAP (*red*) and Pax6 (*green*) immunofluorescence in the NMDA-injured retinas after solvent or DMX-5804 treatment. **c** Quantification of relative Pax6+ pixel intensity in YAP + MG in (**b**). **d** Timeline diagram of the experimental procedures used in **e**. Glast-CreERT2 + /tg;ROSA26R-tdTomato + /tg mice were intraperitoneally injected with Tamoxifen for 5 consecutive days. Then NMDA was intraocularly administered. DMX-5804 was injected every 6 h intraperitoneally from 6 hpi until 3 dpi after NMDA injection. The *purple* triangles represent the time points of the sampling. **e** EdU labeling (*gray*) and Pax6 (*green*)/NeuN (*green*) immunofluorescence in the NMDA-injured retinas after 3 days of DMX-5804 treatment. **f** Quantification of relative Pax6+ pixel intensity in YAP + MG in (**e**). **g** Quantification of the percentage of NeuN+tdTomato+ cells in tdTomato+ cells in **b**–**d**. Scale bars, 20 μm (**b**, **e**). For pixel intensity measurements, levels were given as mean ± SEM ($n = 6$ mice per group; Student's *t*-test). For quantification of NeuN+tdTomato+ cells, levels were given as mean ± SEM ($n = 9$ mice per group; Student's t-test). *$p \le 0.05$, **$p \le 0.01$, ***$p \le 0.001$.

DISCUSSION

In zebrafish, reactive MG take three sequential steps to participate in the process of retinal damage repair: (1) acquisition of stem cell properties after retinal damage and proliferation in response to a variety of growth factors and cytokines; (2) amplification of a small population of progenitors through a process called interkinetic nuclear migration in a Pax6-dependent manner; (3) cell cycle exits and neuronal differentiation[2,42]. Since mammals and zebrafish share the same vertebrate ancestors hundreds of millions of years ago, it is interesting to ask whether mammalian MG retain some hidden regenerative abilities. Here, our results support the claims that MG have the ability to undergo the same process as zebrafish to regenerate neurons, while in the injured adult mouse retina this capability is lost at least partially by YAP inhibition.

The canonical Hippo pathway mediated by MST1/2 has been extensively examined with respect to various biological processes[43,44], whereas the physiological and pathological roles of MAP4Ks-mediated YAP phosphorylation remain largely enigmatic. Here, we showed that MAP4K4/6/7, one class of MAP4Ks that regulate YAP activities, controlled the reprogramming of injury-responsive MG in adult mice. Importantly, to our knowledge, this is the first piece of evidence to demonstrate the functions of MAP4Ks-mediated YAP regulation in the mammalian retina. Even more promising, we found that a small molecule inhibitor DMX-5804, which simultaneously inhibits MAP4K4/6/7[24], could effectively promote MG to proliferate and dedifferentiate into RPC-like cells. Moreover, these MG-derived RPC-like cells could spontaneously transdifferentiate into retinal neurons after drug withdrawal.

Previously, transgenic expression of a phospho-deficient variant of YAP (YAP5SA) were reported to stimulate robust proliferation and reprogramming of MG into a progenitor-like state[19,20]. However, most of the YAP5SA-reprogrammed MG reside in a progenitor-like state and fail to differentiate into neurons due to the constitutively activation of transgenic YAP5SA[45]. Therefore, one key question remaining after those studies was whether MG are able to transdifferentiate into neurons after they have become reprogrammed into RPC-like cells by regulating the Hippo pathway. Thus, our work has pushed one step forward by demonstrating that mammalian MG retain the intrinsic ability to transdifferentiate into retinal neurons after they enter the RPC-like state. Furthermore, our data support the advantages of chemical induction in comparison with genetic manipulations, especially for cells which have to go through multiple transitional states to regenerate tissues. More importantly, our results provide compelling proof-of-principle to support the feasibility of in vivo reprogramming and retinal regeneration by applying a therapeutic intervention based upon use of small molecule chemical cocktails in humans.

RGCs are essential neurons in the retina required for the transmission of encoded visual information from the eye to the brain. However, the inability to regenerate lost or severely degenerated RGCs in mammals, either due to disease or trauma, leads to blindness. In contrast, fish can regenerate their entire retina, including RGCs. Considering the same vertebrate ancestry of fish and mammals, the question of whether RGCs can be regenerated from MG to cure such vision impairments in humans has been a central issue and a quest in the ophthalmic regenerative medicine field for many decades. Some studies have suggested that functional RGCs can be regenerated from MG in vivo by loss of PTBP1[14] or overexpression Math5:Brn3b[15], but the tracing system has raised concerns[46,47]. Recently, co-expressions of bHLH transcription factors Ascl1:Atoh1 have been shown to regenerate RGC-like cells from MG in vivo[16]. However, it remains unknown whether modulating endogenous signaling pathways by small molecule chemicals can transdifferentiate MG into RGCs. To provide answers for this question, we used a small molecule DMX-5804 to activate YAP and reprogram MG into a progenitor-like state in the first step, and then RPC-like MG exhibited the intrinsic ability to differentiate into retinal neurons after drug withdraw. Droplet digital PCR detected the expression of *Ascl1* and *Atoh7* in these cells (Supplementary Fig. 9). To our surprise, we identified a small subset of MG that transdifferentiated into RGC-like cells, expressing RBPMS and βIII-tubulin (Fig. 6 and Supplementary Fig. 12). Based on these findings, we propose that MG indeed retain neuron regenerative abilities, and it is feasible to regenerate retinal neurons in the mammalian retina by using small molecule cocktails, rather than, for example, genetic manipulations.

In addition to DMX-5804, we evaluated another canonical Hippo pathway inhibitor XMU-MP-1, which specifically inhibits MST1/MST2[43]. As expected, intraperitoneal administration of XMU-MP-1 suppressed YAP phosphorylation in a dose- and time-dependent manner in adult murine retinas as well (Supplementary Fig. 14a–f). Moreover, XMU-MP-1 was comparable to DMX-5804 in the ability to promote YAP nuclear translocation in normal mice (Supplementary Fig. 14g–i) and MG proliferation in NMDA-damaged retinas (Supplementary Fig. 15a–d). However, DMX-5804 showed a higher potency than XMU-MP-1 to promote neuron regeneration in long-term fate tracing experiments (Supplementary Fig. 15e–j). To solve these differences, we found that only DMX-5804, but not XMU-MP-1, modulated JNK pathway activities in adult murine retinas (Supplementary Fig. 16). More specifically, DMX-5804 also suppressed JNK phosphorylation in NMDA-damaged retinas (Supplementary Fig. 17). Previously, it has been reported that inhibition of MAP4K4/6/7 is beneficial for neuroprotection by suppressing apoptosis downstream of the JNK signaling cascade[48,49]. Accordingly, the levels of JNK phosphorylation in the NMDA-damaged neuroretinas were significantly elevated relative to those in normal (control) retinas during the first 5 days after NMDA injection (Supplementary Fig. 17). Newborn neurons appeared on the 3rd day after NMDA/DMX-5804 administration (Fig. 4e; Supplementary Fig. 6b, c; Supplementary Fig. 7). Thus, we suspected that elevated JNK activities made fragile newborn retinal neurons susceptible to cell death in NMDA/XMU-MP-1 treated neuroretinas. Moreover, it has been reported that during retinal regeneration, an inflammatory microenvironment affects the survival of newborn neurons in the zebrafish retina[50]. MAP4Ks play diverse roles in immune cell signaling, immune responses,

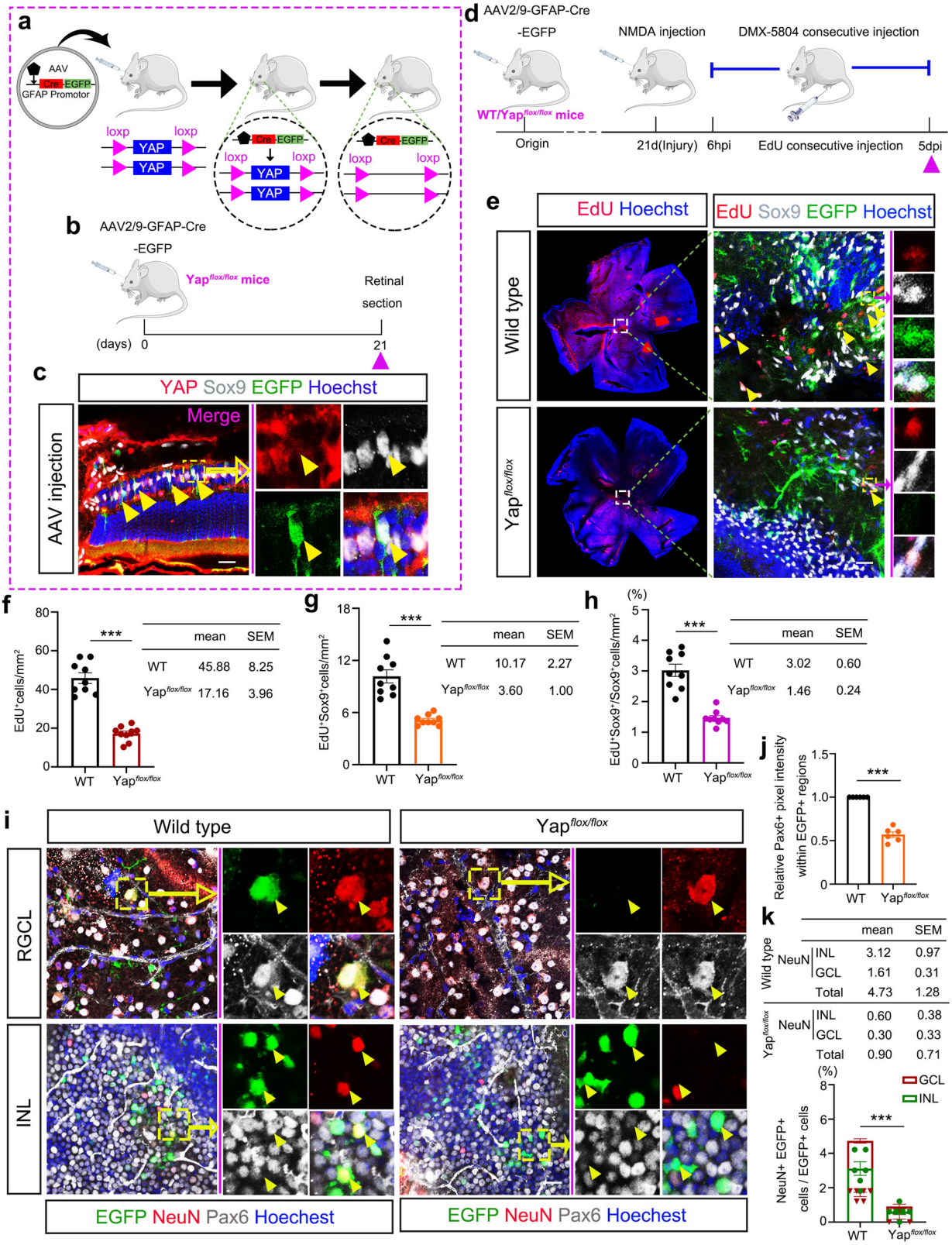

and inflammation[51]. Therefore, DMX-5804 treatment may also relieve the inflammation within the microenvironment and protect neurogenesis in the injured retina by inhibiting the MAPK cascades. However, our observations could not simply be explained by the roles of MAP4Ks in neuronal protection, as both in vitro and in vivo experiments clearly demonstrated their functions in regulating the proliferation and trans-differentiation of MG. Taken together, we propose that multiple targets may work downstream of MAP4K4/6/7 to regulate MG-mediated retinal regeneration. Specifically, intracellular signaling pathways and

Fig. 5 NMDA/DMX-5804 induced MG plasticity is absent in YAP conditional knockout mice. a–c Conditional YAP knockout strategies and representative results. Schematic diagram showing conditional YAP knockout strategies and tracing system in mouse Müller glia using AAVs (**a**, **b**). YAP (*red*), Sox9 (*gray*) and Cre (EGFP) immunofluorescence in mouse retinal sections after pAAV-short GFAP-MCS-EGFP-3FLAG injection (**c**). The *red* triangles represent the time points of the EdU injection and the *purple* triangles represent the time points of the sampling. **d** Timeline diagram of the experimental procedures used in (**e**–**k**). Wild type or $YAP^{flox/flox}$ mice were intravitreally injected with pAAV-GFAP-Cre-T2A-EGFP. NMDA was intraocularly administered 3 wk later. Then DMX-5804 was injected every 6 h intraperitoneally from 6 hpi to 5 dpi after NMDA injection. After that, mice were sacrificed and the retinas were analyzed. **e** EdU labeling (EdU +; *red*) and SOX9 immunofluorescence (SOX9 +; *gray*) on whole flat-mounted retinas infected with pAAV-GFAP-Cre-T2A-EGFP after NMDA injury and DMX-5804 treatment. **f** Quantification of the number of cells positive for EdU labeling (EdU +; *red*) per mm^2 in (**e**). **g** Quantification of the number of cells positive for both EdU labeling (EdU +; *red*) and SOX9 immunofluorescence (SOX9 +; *gray*) per mm^2 in (**e**). **h** Quantification of the percentage of EdU+ SOX9+ cells in SOX9+ cells per mm^2 in (**e**). **i** NeuN (NeuN +; *red*) and Pax6 (Pax6 +; *gray*) immunofluorescence on whole flat-mounted retinas infected with pAAV-GFAP-Cre-T2A-EGFP after NMDA injury and DMX-5804 treatment. **j** Quantification of relative Pax6+ pixel intensity in YAP + MG in (**i**). **k** Quantification of the percentage of NeuN+EGFP+ cells in EGFP+ cells in (**i**). Scale bars, 20 μm (**c**, **e**, **i**). For quantification of EdU+ SOX9+ cells, levels were given as mean ± SEM ($n = 9$ mice per group; Student's *t*-test). *$p \le 0.05$, **$p \le 0.01$, ***$p \le 0.001$. For pixel intensity measurements, levels were given as mean ± SEM ($n = 6$ mice per group; Student's *t*-test). For quantification of NeuN+ EGFP+ cells, levels were given as mean ± SEM ($n = 6$ mice per group; Student's *t*-test).

extracellular microenvironment might work synergistically to enhance the retinal regenerative efficiency of DMX-5804.

MAP4Ks and MST1/2 work in parallel to regulate LATS1/2 phosphorylation, and subsequently YAP phosphorylation[22]. As both DMX-5804 and XMU-MP-1 are functional in vivo, we examined their synergistic effects in MG. Combined treatment of both chemicals further increased the number of proliferative MG in NMDA-treated mice, yet we failed to detect more NeuN+ tdTomato+ cells compared with the mice treated with DMX-5804 (Supplementary Fig. 18). These results also supported our claim that targets other than YAP downstream of MAP4K4/6/7 mediated their functions in retinal regeneration. Recently, new inhibitors of LATS kinases were reported[52,53], and it is interesting to test their efficiency and efficacy in promoting retinal regeneration. However, we suspect that it may not further increase the number of regenerated neurons, considering the fact that multiple targets work downstream of MAP4K4/6/7.

Clinically, a considerable number of patients come to the clinics when they pass the acute phase of retinal injury. Therefore, we were curious about the retinal regenerative capabilities of DMX-5804 when drugs were delivered after the acute phase of retinal damage. It is intriguing to note that DMX-5804 showed higher efficacy than XMU-MP-1 in promoting MG proliferation when both compounds were administrated 2 days post NMDA-induced injury (Supplementary Fig. 19c–f). To interpret this finding, we checked the time course of both canonical and MAP4Ks-mediated Hippo pathway activation after retinal injury, indicated by the phosphorylation level of MOB1 and YAP[43,44]. The phosphorylation levels of both MOB1 and YAP increased sharply within 24 h after retinal damage (Fig. 1a, c, 2b, d; Supplementary Fig. 19a, b). However, MOB1 phosphorylation (pMOB1) was diminished (Supplementary Fig. 19a, b), while YAP phosphorylation remained higher than the normal level 24 h after injury (Fig. 1a, c; Fig. 2b, d), which might serve as an insurance mechanism to prevent proliferative signals from rebounding in mammals. This inconsistency between the phosphorylation levels of MOB1 and YAP might explain the weaker effect of XMU-MP-1 when both compounds were injected after the acute phase (2 dpi) separately. Thus, these results further support the claims that MAP4Ks-mediated YAP phosphorylation might be a more appropriate target for drug development.

The dysregulation of the Hippo pathway and hyperactivation of YAP drive tumorigenesis[54,55], and thus raise safety issues, since DMX-5804 was delivered systematically in our studies. Based on our results, we concluded that DMX-5804 did not affect cell proliferation, cell death or the normal anatomical structure of major organs at the dose we tested (Supplementary Fig. 13). Secondly, the entry of small-molecule drugs into the retina remains a challenge due to the existence of the blood-retinal-barrier (BRB). There are two types of BRBs: the inner BRB (iBRB) formed by non-fenestrated endothelial cells, pericytes and glia cells, and the outer BRB (oBRB) formed by retinal pigment epithelial cells and their tight junctions. Therefore, the size, hydrophilicity and hydrophobicity of the compound affect its permeability into the retina[56,57]. Although another two inhibitors of MAP4K4 (PF-06260933[26] and GNE-495[58]) have an IC_{50} comparable to that of DMX-5804, but their BRB penetration abilities are much lower than DMX-5804. Thirdly, the off-target effects should be taken into consideration as well when developing small-molecule drugs[59,60]. Apart from MAP4K4/6/7, VEGFR was identified as a primary off-target hit of DMX-5804, but is nearly 700-fold less sensitive than MAP4K4[24]. Lastly, the Ames assay demonstrated a mutagenic risk of PF-06260933[26], whereas no detectable mutagenic risk was found for DMX-5804[24]. Taken together, these factors guided our choice of DMX-5804 for animal studies.

Numerous ways have been invented to stimulate MG de-differentiation and trans-differentiation in mammals to date. However, transgenic tools were used in most of those cases[10,13,14]. AAVs, which have high affinities for glial cells, have been used as vectors to express pro-proliferation genes or silence endogenous suppressor genes in the damaged retina to assist the de-differentiation, proliferation and trans-differentiation of MG. However, AAVs have only limited cargo capacity to carry foreign genes[10,61]. As a result, high titers of AAVs expressing various genes or silencing sequences have to be injected intraocularly, since multiple regulatory factors are required to modulate the fate of MG for retinal regeneration, which may also raise biosafety issues[45,61]. To conquer this problem, the combination of multiple small-molecule chemicals targeting endogenous signaling pathways may be a better choice. Here, we showed that the small-molecule compound DMX-5804 promoted adult mouse MG to reprogram, proliferate and spontaneously trans-differentiate into retinal neurons, with a small fraction expressing the markers of amacrine cells and RGCs after retinal damage (Supplementary Fig. 20). However, the conversion efficiency from MG into mature neurons is relatively low in our hands. Therefore, we propose DMX-5804 might be used as one of several ingredients comprising a cocktail therapy for retinal regeneration. Moreover, the development of appropriate carriers for intraocular delivery might further enhance the efficacy of drug combinations and provide more benefits for clinical practice.

METHODS

Animals

Glast-CreERT2 + /tg;ROSA26R-tdTomato$^+$/tg mice were from a mix of Glast-CreERT2$^+$/tg C57BL/6 J and ROSA26R-tdTomato$^+$/tg C57BL/6 J mice. Males and females were both used in experiments. All in vivo experiments were performed on adult mice that were at least 40 days old. The mice were euthanized with 60% carbon dioxide before sampling. All animals were housed in

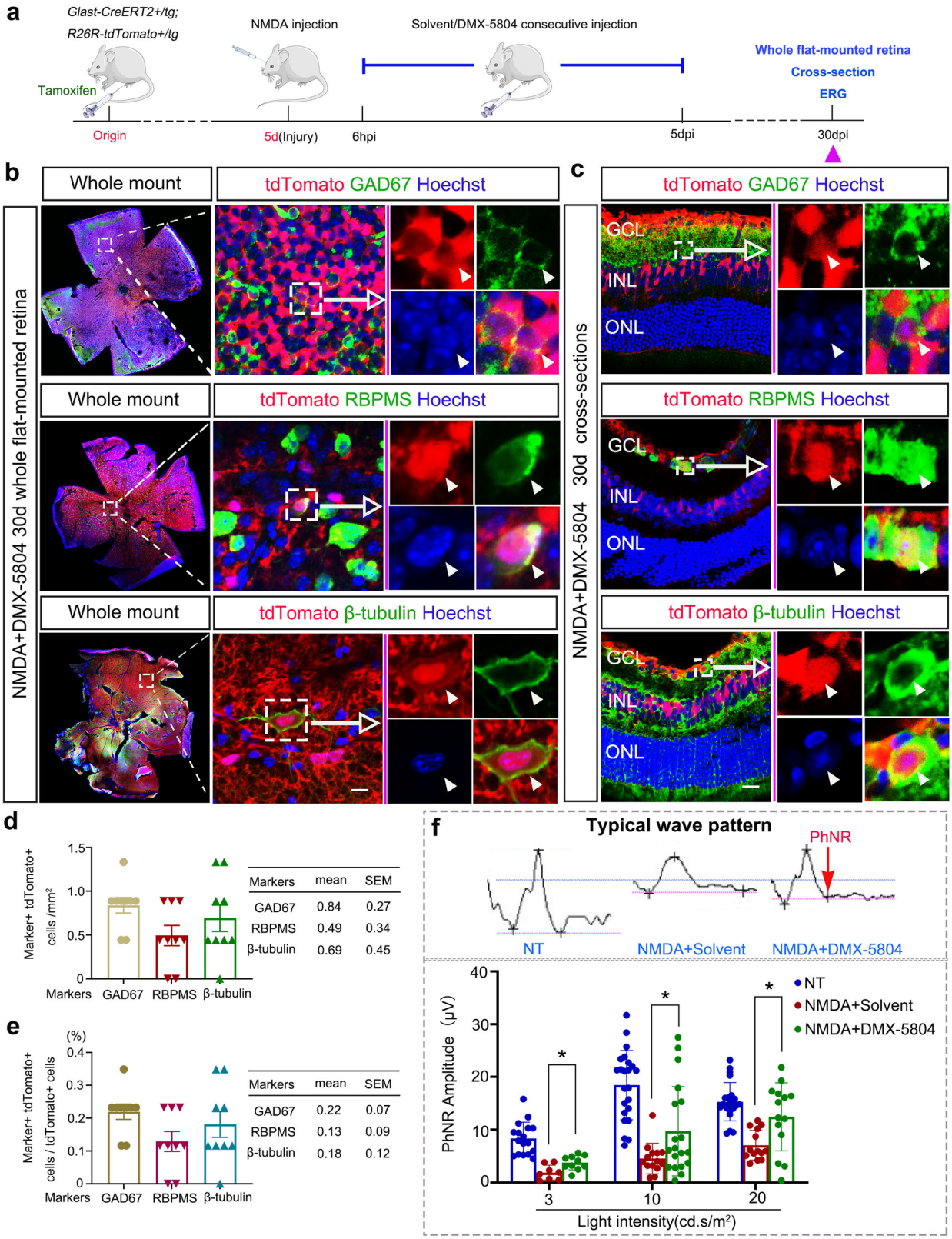

Xiamen University Laboratory Animal Center; all procedures were approved by the Xiamen University Institutional Animal Care and Use Committee (IACUC) and complied with the ARVO Statement for the Use of Animals in Ophthalmic and Vision Research.

MIO-MI cells

MIO-MI cells (RRID: CVCL_0433) were a kind gift from Wenzhou Medical University. The cells were maintained in DMEM containing 10% fetal bovine serum and Penicillin/Streptomycin. For all

Fig. 6 Long-term tracing of MG Fate after NMDA/DMX-5804 Treatment. a Timeline diagram of the experimental procedures used in **b**–**d**. Glast-CreERT2 + /tg;ROSA26R-tdTomato + /tg mice were intraperitoneally injected with Tamoxifen for 5 consecutive days. Then NMDA was intraocularly administered. DMX-5804 was injected every 6 h intraperitoneally from 6 hpi until 5 dpi after NMDA injection. Thirty (30) days after NMDA injection, mice were sacrificed and retinal samples were analyzed. The *purple* triangles represent the time points of the sampling. **b** GABAergic cell marker GAD67 (*green*) or retinal ganglion cell marker (RBPMS/βIII-tubulin, *green*) immunofluorescence on whole flat-mounted NMDA-injured retinas after DMX-5804 treatment. **c** GABAergic cell marker GAD67 (*green*) or retinal ganglion cell marker (RBPMS/βIII-tubulin, *green*) immunofluorescence on retinal sections after DMX-5804 treatment. **d** Quantification of the number of GAD67+tdTomato+ cells, RBPMS+ tdTomato+ cells and βIII-tubulin+ tdTomato, per mm^2 in (**b**, **c**). **e** Quantification of the percentage of GAD67+tdTomato+ cells, RBPMS+ tdTomato+ cells and βIII-tubulin+ tdTomato+ in tdTomato+ cells in **b** and **c**. **f** Illustrative waveforms of PhNR tests and the quantification of PhNR signal strengths after DMX-5804 treatment. Scale bars, 20 μm (**b**, **c**). For quantification of Neuronal marker+ tdTomato+ cells, levels were given as mean ± SEM ($n = 9$ mice per group). For quantification of PhNR signal strengths, results were given as mean ± SEM ($n = 10$ mice per group; Student's *t*-test). *$p \le 0.05$, **$p \le 0.01$, ***$p \le 0.001$.

treatments, 6.0×10^5 cells per well were seeded into 6-well plates. For siRNA experiments, MIO-M1 cells were transfected using the RNAFit according to the instructions (HANBIO). MAP4K4 and NC siRNA (HH20201222FJCJY-SI01), MAP4K6 and NC siRNA (HH20201222FJCJY-SI02), MAP4K7 and NC siRNA (HH20201222FJCJY-SI03) were synthesized at HANBIO (Shanghai, China). For small-molecule inhibitors treatment, cells were treated with different concentration of DMX-5804 (Cat. No. HY-111754, MedChemExpress). Subsequently, a proper concentration was selected to verify time-dependent effects of DMX-5804.

AAV production and intravitreal injection

AAV2/9-GFAP-CRE-EGFP and AAV2/9-Syn-Gcamp6s was synthesized at HANBIO (Shanghai, China). AAV2/8-short-GFAP-EGFP was synthesized at OBIO technology (Shanghai, China). Mice were first anesthetized through intraperitoneal injection of pentobarbital sodium (1% in PBS). Tropicamide (0.5%) was then topically administered for pupillary dilation. While applying gentle pressure around the eye socket to extrude the eye, a 33-gauge needle was passed through the sclera just behind the limbus, into the vitreous cavity. Injection of 2 μl of AAV was made with direct observation of the needle in the center of the vitreous cavity. For NMDA intravitreal injection, injection of 2 μl of NMDA (100 mM, Cat. No. M3262-25mg, Sigma Aldrich) was made in the center of the vitreous cavity.

The Compounds preparation and intraperitoneal injection

DMX-5804, XMU-MP-1 and verteporfin were dissolved in solvent with the order: 10% DMSO, 40% PEG300, 5% Tween-80 and 45% PBS for mother solution. DMX-5804, XMU-MP-1 and the solvent control were each administered by intraperitoneal injection, as 2 mg/kg dose, 6 h apart for different consecutive days according to experimental designs, while verteporfin and the solvent control were each administered by intraperitoneal injection, as 2 mg/kg dose, 6 h apart but with 1 h interval before DMX-5804 injection. To label cells in S phase, 5-ethynyl-2′-deoxyuridine (EdU) (APExBIO, Cat. No. B8337) was injected intraperitoneally at a concentration of 50 mg/kg body weight and mice were euthanized by cervical dislocation 12 or 24 h later.

Western blotting

For cells, the culture medium was removed and cells were briefly washed in PBS containing protease (Thermo Fisher Scientific, Cat. No.1862209) and phosphatase inhibitors (Thermo Fisher Scientific, Cat. No.78420). Cells were lysed using a cold lysis buffer (Thermo Fisher Scientific, Cat. No.1861603) containing protease and phosphatase inhibitors and the cells were flash-frozen and kept at −80 °C until used.

For retinas, neural retinas were dissected in PBS and briefly washed in PBS containing protease and phosphatase inhibitors. Samples were put into ice-cold lysis buffer containing protease and phosphatase inhibitors and the retinas were flash-frozen (liquid nitrogen) and then stored at −80 °C until used.

For protein extraction, samples were thawed on ice for 10 min in lysis buffer containing protease and phosphatase inhibitors, then cells or retinas were homogenized and centrifuged at 4 °C (2000 rpm, 10 min), and the supernatants were transferred to a new tube. Clarified protein lysates were quantified by the Bradford assay.

For Western blotting, 20 mg protein was loaded onto 8–10% SDS-PAGE gels for electrophoresis and subsequently transferred (90 V, 2–3 h) onto PVDF western blotting membranes (Roche, Cat. No. 3010040001) using the Criterion™ System BioRad. Membranes were washed in TBST pH 7.4 (20 mM Tris, 137 mM NaCl, 0.1% Tween 20) and blocked for 1 h at room temperature (RT) with 5% non-fat milk in TBST to reduce non-specific antibody binding. At least 3 independent controls and treated samples were probed with the following primary antibodies (in 5% milk, overnight at 4 °C): YAP (1:500, Cell signaling Tec., Cat. No. 14074, RRID: AB_2650491), p YAP (1:2000, Cell signaling Tec., Cat. No. 13008, RRID: AB_2650553), LATS1 (1:1000, CST, Cat. No. #3477, RRID: AB_2133513), Phospho-LATS1 (1:1000, CST, Cat. No. #8654, RRID: AB_10971635), MAP4K4 (1:500, Cell Signaling Tec., Cat. No. #3485, RRID: AB_2140972), MAP4K6 (1:500, Novus, Cat. No. NBP1-22989, RRID: AB_1726507) and MAP4K7 (1:500, Genetex, Cat. No. GTX13141, RRID: AB_383061), JNK (1:1000, CST, Cat. No. #9252, RRID: AB_2250373), Phospho-JNK (1:1000, CST, Cat. No. #4668, RRID: AB_2869284), MOB1 (1:1000; Cell signaling Tec., Cat. No. 13730, RRID: AB_2783010), p MOB1 (1:1000, Cell signaling Tec., Cat. No. #8699, RRID: AB_11139998). Vinculin (1:5000, Cell Signaling Tec., Cat. No. 13901, RRID: AB_2728768) was used as loading control. After primary antibody incubation, membranes were washed in TBS-T, incubated with HRP-conjugated secondary antibodies (1-h, RT), detected with Clarity™ Western ECL Substrate (Bio-Rad, Cat. No. 170-5060) and imaged with the Chemidoc Touch Imager (Bio-Rad Laboratories Inc, Hercules, CA, USA). Uncropped Western blotting images were provided in Supplementary Fig. 21, where the size markers were labeled. All blots were processed in parallel and derive from the same experiment.

Immunofluorescence staining on cells

MIO-M1 cells seeded in 6-well culture plates were fixed in 4% paraformaldehyde (PFA) in PBS for 10 min. The PFA was removed, and the plates were washed with PBS. Fixed cells were treated with blocking buffer containing 2% BSA in PBS for 1 h on ice. Plates were incubated for 24 h in primary antibodies in a humidified chamber. The following antibodies and concentrations were used: Glutamine Synthetase (1:500, Millipore, Cat. No. MABN1182, RRID: AB_2110656), GFAP (1:500, Millipore, Cat. No. G6171, RRID:AB_1840893), MAP4K4 (1:500; Cell Signaling Tec., Cat. No. 3485, RRID: AB_2140972), MAP4K6 (1:500; Novus, Cat. No. NBP1-22989, RRID: AB_1726507) and MAP4K7 (1:500; Genetex, Cat. No. GTX13141, RRID: AB_383061), YAP (1:100, Santa Cruz, Cat. No. 101199, RRID: AB_1131430), ki67 (1:500, Abcam, Cat. No. ab16667,

RRID: AB_302459), HuC/D (1:500, Abcam, Cat. No. ab184267, RRID: AB_2864321). After washing with PBS, anti-mouse (488, 1:300, Thermo Fisher Scientific, Cat. No. A21022, RRID: AB_141607) or anti-rabbit (488, 1:300, Thermo Fisher Scientific, Cat. No. A11008, RRID: AB_143165 or 594, 1:300, Thermo Fisher Scientific, Cat. No. A11012, RRID: AB_141359) secondary antibodies were applied, and signals were visualized using a Zeiss LSM 880+Airyscan.

Immunofluorescence staining on tissue sections

For the paraffin sections, enucleated eyes were immersed in 4% paraformaldehyde (PFA) in 0.1 M PBS overnight at room temperature (RT), corneas and lenses were removed. After fixation, eyecups were administered tissue dehydration in accordance to the order: 70% ethyl alcohol (2 h), 80% ethyl alcohol (1 h), 95% ethyl alcohol (1 h), 100% ethyl alcohol (1 h, with 3 repeats), xylene (30 min, with 3 repeats), dehydrated samples were embedded with paraffin at 60 °C (1 h, with 3 repeats), and then mounted in paraffin tissue molds and stored at RT before sectioning. Paraffin sections were cut at 8 µm thickness on a microtome and mounted on Superfrost Plus slides (CITOTEST, Cat. No. 188105). Before immunofluorescence, slides were dewaxed in accordance to the order: xylene (15 min, 2 repeats), 100% ethyl alcohol (10 min), 95% ethyl alcohol (5 min), 80% ethyl alcohol (5 min), 70% ethyl alcohol (5 min) and antigen-retrieval was performed in antigen retrieval buffer (3 g sodium citrate and 0.4 g citric acid in 1 L deionized water) at 100 °C for 20 min. For EdU, sections were permeabilized for 30 min in 0.5% Titron-X100 diluted in 0.1 M PBS, and then washed using 3%BSA diluted in 0.1 M PBS. The Click-iT EdU Alexa Fluor® 594 (Thermo Fisher Scientific, Cat. No.C10639) was used following the manufacturer's instructions.

For the cryosections, enucleated eyes were immersed in 4% PFA in 0.1 M PBS for 1 h at RT, corneas and lenses were removed. After fixation, eyecups were washed in PBS 3 times for 10 min on ice, and then cryoprotected by immersing in 30% sucrose until the tissues sank to the bottom of the tubes. Then, tissues were embedded in O.C.T. for 15–20 min and then flash-frozen in liquid nitrogen and stored at −80 °C before sectioning. Cryosections were cut at 20 µm thickness on a cryostat and mounted on Superfrost Plus slides (CITOTEST, Cat. No. 188105).

For immunofluorescence, sections were rinsed with PBS and incubated for 2 h at 4 °C with 2% bovine serum albumin (BSA), and 0.5% Triton X-100 diluted in 0.1 M PBS (pH 7.4). Slides were incubated for 24 h in primary antibodies in a humid chamber. The following antibodies and concentrations were used: YAP (1:100, Santa Cruz, Cat. No. 101199, RRID: AB_1131430), SOX9 (1:500, Abcam, Cat. No. ab185966, RRID: AB_2728660), GFAP (1:500, Millipore, Cat. No. G6171, RRID:AB_1840893), Pax6 (1:500, Santa Cruz, Cat. No. sc81649, RRID: AB_1127044), Pax6 (1:500, Abcam, Cat. No. ab195045, RRID: AB_2750924), NeuN (1:500, Novus, Cat. No. NBP1-92693, RRID: AB_11036146), NeuN (1:500, Abcam, Cat. No. ab177487, RRID: AB_2532109), GAD67 (1:100, Abcam, Cat. No. ab26116, RRID: AB_448990), RBPMS (1:500, Proteintech, Cat. No. 15187-1-AP, RRID: AB_2238431), βIII-tubulin (1:500, Abcam, Cat. No. ab18207, RRID: AB_444319), ki67 (1:500, Abcam, Cat. No. ab16667, RRID: AB_302459), PCNA (1:500, CST, Cat. No. #13110, RRID: AB_2636979), HuC/D (1:500, Abcam, Cat. No. ab184267, RRID: AB_2864321), Calretinin (1:200, Abcam, Cat. No. ab92341, RRID: AB_2049245), MAP2 (1:200, Abcam, Cat. No. ab183830, RRID: AB_2895301), Recoverin (1:20, Proteintech, Cat. No. 10073-1-AP, RRID: AB_2178005), Rhodopsin (1:200, ABclonal, Cat. No. A7245, RRID: AB_2863548), Arrestin (1:200, Millipore, Cat. No. AB15282, RRID: AB_1163387). Next, slides were rinsed 3 times in PBS and blocked for 30 min in 2% BSA, and 0.5% Triton X-100 diluted in 0.1 M PBS (pH 7.4) before incubation in secondary antibodies. Anti-mouse (488, 1:300, Thermo Fisher Scientific, Cat. No. A21022, RRID: AB_141607 or 594, 1:300, Thermo Fisher Scientific, Cat. No. A11032, RRID: AB_2534091) or anti-rabbit (Alexa Fluor-488, 1:300, Thermo Fisher Scientific, Cat. No. A11008, RRID: AB_143165 or Alex Fluor-594, 1:300, Thermo Fisher Scientific, Cat. No. A11012, RRID: AB_141359) secondary antibodies were applied and incubated for 1 h in the dark at RT. Hoechst 33342 (1:2000, Thermo Fisher Scientific, Cat. No. H3570) was included in the secondary antibody solution at a 1:2000 concentration. After incubation with secondary antibodies, slides were rinsed 3 times in PBS. Slides were coverslipped with VECTASHIELD® antifade mounting medium (Vector Labs, Cat. No. H-1000-10). Retinal sections from controls and treated mice were immunolabeled in parallel to insure identical processing.

EdU staining and immunofluorescence on whole mount

Immunostaining on whole mount was performed using standard procedures with the following modifications: (i) enucleated eyes were immersed in 4% PFA in 0.1 M PBS for 1 h at RT, then retinas were isolated from the eyecup, and incised radially into four radial pieces; (ii) the retinas were first incubated overnight in a blocking solution containing 2% BSA and 0.5% Triton X-100 in PBS (pH 7.4); (iii) For EdU, retinas were washed using 3% BSA diluted in 0.1 M PBS. The Click-iT EdU Alexa 488 (Thermo Fisher Scientific, Cat. No.C10638), Click-iT EdU Alexa 594 (Thermo Fisher Scientific, Cat. No.C10639), or Click-iT EdU Alexa 647 (Thermo Fisher Scientific, Cat. No.C10640) was used following the manufacturer's instructions. (iii) The retinas then were incubated in a mixture of primary antibodies. The following antibodies and concentrations were used: SOX9 (1:500, Abcam, Cat. No. ab185966, RRID: AB_2728660), NeuN (1:500, Abcam, Cat. No. ab177487, RRID: AB_2532109), GAD67 (1:100, Abcam, Cat. No. ab26116, RRID: AB_448990), RBPMS (1:500, Proteintech, Cat. No. 15187-1-AP, RRID: AB_2238431), βIII-tubulin (1:500, Abcam, Cat. No. ab18207, RRID: AB_444319). Nuclei were counterstained with 1:2000 Hoechst (1:2000, Thermo Fisher Scientific, Cat. No. H3570). Next, retinas were rinsed 3 times in PBS and blocked for 30 min in 2% BSA, and 0.5% Triton X-100 diluted in 0.1 M PBS (pH 7.4) before incubation in secondary antibodies. 1:300 dilutions of Alexa Fluor 488 or 594 conjugated secondary antibodies (antibodies were from Thermo Fisher Scientific which has been described above) were applied and incubated for 1 h in the dark at room temperature. Hoechst was included in the secondary antibody solution at a 1:2000 dilution. Finally, Slides were coverslipped with VECTASHIELD® antifade mounting medium (Vector Labs, Cat. No. H-1000-10) on Superfrost Plus slides (CITOTEST, Cat. No. 188105) before observation.

Fluorescence-activated cell sorting (FACS)

Following euthanasia, retinas were dissociated with Papain/DNase for 30 min at 37 °C. The tissue was then gently triturated for adequate dissociation before Ovomucoid was added. Suspending cells were spun down at 300 g and then resuspended in Neurobasal/Ovomucoid/ DNase solution and passed through a 35 microns filter. FACS was then performed on a MoFlo Astrios EQS (Beckman).

RNA extraction and droplet digital PCR

The RNeasy Plus Micro Kit (cat. no. 74034, QIAGEN) was used for RNA extraction from isolated MG. Total mRNA was reverse transcribed in the presence of PrimeScript™ RT reagent Kit with gDNA Eraser (Perfect Real Time) (Takara, Cat. No. RR047B). Droplet digital PCR was used to measure the levels of transcription factors in isolated MG following a previous method (Fisher et al., 2015). The primers used to amplify the cDNA sequences were *Ascl1* (Forward: 5′-GAACTGATGCGCTGCAAAC-3′; Reverse 5′-CGTCTCCA CCTTGCTCATCT-3′); *Atoh1* (Forward: 5′-CCACAGCTTCCTGCAAA AAT -3′; Reverse: 5′-GAGTAACCCCCAGAGGAAGC-3′): *Atoh7* (Forward: 5′- AGTGGGGCCAGGACAAGA-3′; Reverse: 5′-GGGTCTACCTG GAGCCTAGC-3′); *Brn3b* (Forward: 5′-CAGCAGTTCCAGCAGCAGT-3′;

Reverse: 5′-ATGGTGGTGGTGGCTCTTAC-3′); *Isl1* (Forward: 5′-AGC TGGAGACCCTCTCAGTC-3′; Reverse: 5′-TGCTTCTCGTTGAGCACAG T-3′). PCR was run using PerfeCta Multiplex qPCR ToughMix (Quanta Biosciences, Gaithersburg, MD, USA). Droplet digital PCR was performed on a Naica Crystal Digital PCR system™ (Stilla Technonologies, Villejuif, France). Stilla's Crystal Miner® software was used to measure the droplet identification and fluorescence intensity.

Primary MG cell culture

Neuroretinas from Glast-CreERT2 + /tg;ROSA26R-tdTomato + /tg mice were harvested and incubated in papain/DNase solution (Worthington) for 30 min at 37 °C. Afterwards, cell mixtures were triturated and an equal volume of ovomucoid was added to stop the papain reaction (Worthington). The dissociated cells were then spun at 300 g at room temperature, and resuspended in Neurobasal medium with 10% FBS (Clontech), 100 ng/mL mEGF (R&D systems), 1 mM L-glutamine (Invitrogen), N2 (Invitrogen) and 1% Penicillin-Streptomycin (Invitrogen). Cells from 6 retinas were plated into a 12-well culture plate, and cultured at 37 °C. Culture media was changed every other day until confluent monolayers of MG were reached. At day 7, P1 primary MG cells were infected with MAP4K4/6/7 siRNA or Control siRNA and the immunofluorescence was performed after 5 days.

Histopathology (H&E staining)

Organs collected from mice treated with solvent or DMX-5804 were embedded in paraffin after paraformaldehyde fixation and tissue dehydration. The paraffin blocks were cut into sections with 6 µm thickness, and then stained with hematoxylin and eosin, using conventional histopathology methods.

TUNEL Assay

TUNEL assay was performed using DeadEnd Fluorometric TUNEL System (Promega, G3250). Frozen sections of organs were rehydrated and incubated with Proteinase K in Tris/HCl (pH = 7.4,10 mM) for 30 min at 37 °C. The tissue sections were washed with PBS for 5 min for 3 times, 50 µL of TUNEL reaction mixture was added on the sections and the sections were placed in dark for 1 hour at 37 °C, followed by washing 3 times with PBS for 5 min each. Finally, the specimens were counterstained with Hoechst, mounted, and photographed with a microscope (DM2500; Leica Microsystems).

Imaging

Confocal images were acquired using a Zeiss LSM 880+Airyscan. For standardization between samples, all images were acquired with the same laser power, detector gain, scan speed, and pinhole size. Z stack images with an identical step-size and thickness were acquired for each retinal section and a maximal intensity projection were obtained.

Measurement of photopic negative response (PhNR)

PhNR was recorded as previously described in ref. [40]. Light stimuli were delivered via a Ganzfeld unit from white light–emitting diodes. Light energies were calibrated as luminance energy units in candela seconds per meter squared (cd.s/m^2). Photopic responses to three different stimulus strengths between 3 and 20 cd.s/m^2 were presented on a 40.0 cds/m^2 rod-saturating green background. Amplitudes of the PhNR were initially measured by taking the amplitude at a fixed criterion time after the stimulus onset, again with respect to baseline. The trough was identified following b wave and obtained calculating the amplitude from baseline to trough. Measurement results using both forms of amplitude analysis were comparable for data presentation.

Quantification and statistical analysis

For all figure panels, images were imported into Adobe Photoshop CS software for identical and minimal processing. For each control, mutant, or treated experimental group, three to six independent retinas from different mice were examined and the results presented in the manuscript are representative images from at least three separate experiments. A Student's *t*-test was used to compare measurements between controls and mutant mice. *P*-values < 0.05 were considered as statistically significant.

Quantifications of the number of labeled cells in stretched preparation of mouse retinas were calculated from 5 different fields of per retina and using 3 retinas per condition.

For quantification of nuclear YAP immunofluorescence, ZEN2.3 lite software (Carl Zeiss IMT Co. Ltd. Germany) was used to quantify YAP pixel intensities when coincident with $SOX9^+$ pixels (to denote nuclear localization). For EdU quantification of confocal images, EdU^+ cells were manually counted in each image and retinal area was measured in ZEN2.3 lite software to determine EdU^+ cells per mm^2. To measure pixel co-localization across MG within a given retina ZEN2.3 lite software was used to plot pixel intensities along a line drawn across the image and Pearson's Correlation Coefficient (R) was calculated. For quantification of relative pixel intensity per mm^2, total pixel intensity was measured in ZEN2.3 lite software and divided by the total area of each image.

For quantification of western blotting, images were taken with the Chemidoc Touch Imager (Bio-Rad Laboratories Inc, Hercules, CA, USA) and scanned at high-resolution for protein band size and signal intensity. Densitometry measurements were obtained using the Image LabTM software (Bio-Rad Laboratories Inc, Hercules, CA, USA). All bands were normalized to their corresponding loading controls. The results shown are from at least 3 biological replicates. The Student's *t*-test was used to determine differences between mutants and controls; the threshold for statistical significance was set as *p*-values < 0.05.

For quantification of mRNA by qPCR, each q-RT-PCR reaction was performed in triplicate for each independent control ($n = 3$) or treatment group ($N = 3$) cDNA samples. The mean ΔΔCT values were normalized against the housekeeping genes 18 s rRNA and corresponding ΔΔCT values were $\log_2$-transformed to obtain fold change values. For data analysis, the Student's *t*-test was used to determine relative gene expression ratios and a *p*-value of <0.05 was considered as statistically significant. GraphPad Prism version 9.0 software (GraphPad Software Inc., San Diego, CA, USA) was applied for data processing and statistically analysis.

Reporting summary

Further information on research design is available in the Nature Research Reporting Summary linked to this article.

DATA AVAILABILITY

All data supporting the conclusions of this study are either provided in this published paper (and its Supplementary Information files) or available from the authors upon reasonable request.

Received: 5 October 2022; Accepted: 27 June 2023;
Published online: 13 July 2023

REFERENCES

1. Stern, J. H. et al. Regenerating eye tissues to preserve and restore vision. *Cell Stem Cell* **22**, 834–849 (2018).
2. Goldman, D. Müller glial cell reprogramming and retina regeneration. *Nat. Rev. Neurosci.* **15**, 431–442 (2014).
3. Hamon, A., Roger, J. E., Yang, X. J. & Perron, M. Müller glial cell-dependent regeneration of the neural retina: An overview across vertebrate model systems. *Dev. Dyn.* **245**, 727–738 (2016).

4. Langhe, R. et al. Müller glial cell reactivation in Xenopus models of retinal degeneration. *Glia* **65**, 1333–1349 (2017).
5. Singhal, S. et al. Human Müller glia with stem cell characteristics differentiate into retinal ganglion cell (RGC) precursors in vitro and partially restore RGC function in vivo following transplantation. *Stem Cells Transl. Med.* **1**, 188–199 (2012).
6. Liu, Y., Wang, C. & Su, G. Cellular Signaling in Müller Glia: Progenitor Cells for regenerative and neuroprotective responses in pharmacological models of retinal degeneration. *J. Ophthalmol.* **2019**, 5743109 (2019).
7. Dyer, M. A. & Cepko, C. L. Control of Müller glial cell proliferation and activation following retinal injury. *Nat. Neurosci.* **3**, 873–880 (2000).
8. Joly, S., Pernet, V., Samardzija, M. & Grimm, C. Pax6-positive Müller glia cells express cell cycle markers but do not proliferate after photoreceptor injury in the mouse retina. *Glia* **59**, 1033–1046 (2011).
9. Bernardos, R. L., Barthel, L. K., Meyers, J. R. & Raymond, P. A. Late-stage neuronal progenitors in the retina are radial Müller glia that function as retinal stem cells. *J. Neurosci.* **27**, 7028–7040 (2007).
10. Yao, K. et al. Restoration of vision after de novo genesis of rod photoreceptors in mammalian retinas. *Nature* **560**, 484–488 (2018).
11. Ueki, Y. et al. Transgenic expression of the proneural transcription factor Ascl1 in Müller glia stimulates retinal regeneration in young mice. *Proc. Natl. Acad. Sci. USA.* **112**, 13717–13722 (2015).
12. Jorstad, N. L. et al. Stimulation of functional neuronal regeneration from Müller glia in adult mice. *Nature* **548**, 103–107 (2017).
13. Hoang, T. et al. Gene regulatory networks controlling vertebrate retinal regeneration. *Science* **370**, https://doi.org/10.1126/science.abb8598 (2020).
14. Zhou, H. et al. Glia-to-Neuron Conversion by CRISPR-CasRx Alleviates symptoms of neurological disease in mice. *Cell* **181**, 590–603.e516 (2020).
15. Xiao, D. et al. In vivo regeneration of ganglion cells for vision restoration in mammalian retinas. *Front. Cell Dev. Biol.* **9**, 755544 (2021).
16. Todd, L. et al. Efficient stimulation of retinal regeneration from Müller glia in adult mice using combinations of proneural bHLH transcription factors. *Cell Rep.* **37**, 109857 (2021).
17. Zheng, Y. & Pan, D. The hippo signaling pathway in development and disease. *Dev Cell* **50**, 264–282 (2019).
18. Wu, Z. & Guan, K. L. Hippo signaling in embryogenesis and development. *Trends Biochem. Sci.* **46**, 51–63 (2021).
19. Hamon, A. et al. Linking YAP to Müller Glia quiescence exit in the degenerative retina. *Cell Rep.* **27**, 1712–1725.e1716 (2019).
20. Rueda, E. M. et al. The hippo pathway blocks mammalian retinal müller glial cell reprogramming. *Cell Rep.* **27**, 1637–1649.e1636 (2019).
21. Zhou, D. et al. Mst1 and Mst2 maintain hepatocyte quiescence and suppress hepatocellular carcinoma development through inactivation of the Yap1 oncogene. *Cancer Cell* **16**, 425–438 (2009).
22. Meng, Z. et al. MAP4K family kinases act in parallel to MST1/2 to activate LATS1/2 in the Hippo pathway. *Nat. Commun.* **6**, 8357 (2015).
23. Meng, Z., Moroishi, T. & Guan, K. L. Mechanisms of Hippo pathway regulation. *Genes Dev.* **30**, 1–17 (2016).
24. Fiedler, L. R. et al. MAP4K4 Inhibition Promotes Survival of Human Stem Cell-Derived Cardiomyocytes and Reduces Infarct Size In Vivo. *Cell Stem Cell* **24**, 579–591.e512 (2019).
25. Hamon, A. et al. Retinal Degeneration Triggers the Activation of YAP/TEAD in Reactive Müller Cells. *Invest Ophthalmol. Vis. Sci.* **58**, 1941–1953 (2017).
26. Ammirati, M. et al. Discovery of an in vivo tool to establish proof-of-concept for MAP4K4-based antidiabetic treatment. *ACS Med. Chem. Lett.* **6**, 1128–1133 (2015).
27. Bringmann, A. et al. Müller cells in the healthy and diseased retina. *Prog. Retin. Eye Res.* **25**, 397–424 (2006).
28. Powell, C., Cornblath, E., Elsaeidi, F., Wan, J. & Goldman, D. Zebrafish Müller glia-derived progenitors are multipotent, exhibit proliferative biases and regenerate excess neurons. *Sci. Rep.* **6**, 24851 (2016).
29. Wan, J., Ramachandran, R. & Goldman, D. HB-EGF is necessary and sufficient for Müller glia dedifferentiation and retina regeneration. *Dev Cell* **22**, 334–347 (2012).
30. Karl, M. O. et al. Stimulation of neural regeneration in the mouse retina. *Proc. Natl. Acad. Sci. USA* **105**, 19508–19513 (2008).
31. Fischer, A. J. & Reh, T. A. Müller glia are a potential source of neural regeneration in the postnatal chicken retina. *Nat. Neurosci.* **4**, 247–252 (2001).
32. Hitchcock, P. F., Macdonald, R. E., VanDeRyt, J. T. & Wilson, S. W. Antibodies against Pax6 immunostain amacrine and ganglion cells and neuronal progenitors, but not rod precursors, in the normal and regenerating retina of the goldfish. *J. Neurobiol.* **29**, 399–413 (1996).
33. Osakada, F. et al. Wnt signaling promotes regeneration in the retina of adult mammals. *J. Neurosci.* **27**, 4210–4219 (2007).
34. Lahne, M., Li, J., Marton, R. M. & Hyde, D. R. Actin-Cytoskeleton- and Rock-Mediated INM Are Required for Photoreceptor Regeneration in the Adult Zebrafish Retina. *J Neurosci* **35**, 15612–15634 (2015).
35. Yu, F. X. & Guan, K. L. The Hippo pathway: regulators and regulations. *Genes Dev.* **27**, 355–371 (2013).
36. Wu, F. et al. Single cell transcriptomics reveals lineage trajectory of retinal ganglion cells in wild-type and Atoh7-null retinas. *Nat. Commun.* **12**, 1465 (2021).
37. Rodriguez, A. R., de Sevilla Müller, L. P. & Brecha, N. C. The RNA binding protein RBPMS is a selective marker of ganglion cells in the mammalian retina. *J. Comp. Neurol.* **522**, 1411–1443 (2014).
38. Jiang, S. M. et al. β-III-Tubulin: a reliable marker for retinal ganglion cell labeling in experimental models of glaucoma. *Int. J. Ophthalmol.* **8**, 643–652 (2015).
39. Yao, K. et al. Wnt Regulates Proliferation and Neurogenic Potential of Müller Glial Cells via a Lin28/let-7 miRNA-Dependent Pathway in Adult Mammalian Retinas. *Cell Rep.* **17**, 165–178 (2016).
40. Chrysostomou, V. & Crowston, J. G. The photopic negative response of the mouse electroretinogram: reduction by acute elevation of intraocular pressure. *Invest. Ophthalmol. Vis. Sci.* **54**, 4691–4697 (2013).
41. Locri, F., Cammalleri, M., Dal Monte, M., Rusciano, D. & Bagnoli, P. Protective Efficacy of a Dietary Supplement Based on Forskolin, Homotaurine, Spearmint Extract, and Group B Vitamins in a Mouse Model of Optic Nerve Injury. *Nutrients* **11**, https://doi.org/10.3390/nu11122931 (2019).
42. Wan, J. & Goldman, D. Retina regeneration in zebrafish. *Curr. Opin. Genet. Dev.* **40**, 41–47 (2016).
43. Fan, F. et al. Pharmacological targeting of kinases MST1 and MST2 augments tissue repair and regeneration. *Sci. Transl. Med.* **8**, 352ra108 (2016).
44. Fu, V., Plouffe, S. W. & Guan, K. L. The Hippo pathway in organ development, homeostasis, and regeneration. *Curr. Opin. Cell Biol.* **49**, 99–107 (2017).
45. Martin, J. F. & Poché, R. A. Awakening the regenerative potential of the mammalian retina. *Development* **146**, https://doi.org/10.1242/dev.182642 (2019).
46. Wang, L. L. et al. Revisiting astrocyte to neuron conversion with lineage tracing in vivo. *Cell* **184**, 5465–5481.e5416 (2021).
47. Hoang, T. et al. Genetic loss of function of Ptbp1 does not induce glia-to-neuron conversion in retina. *Cell Rep.* **39**, 110849 (2022).
48. Larhammar, M., Huntwork-Rodriguez, S., Rudhard, Y., Sengupta-Ghosh, A. & Lewcock, J. W. The Ste20 Family Kinases MAP4K4, MINK1, and TNIK Converge to Regulate Stress-Induced JNK Signaling in Neurons. *J. Neurosci.* **37**, 11074–11084 (2017).
49. Bos, P. H. et al. Development of MAP4 Kinase Inhibitors as Motor Neuron-Protecting Agents. *Cell Chem. Biol.* **26**, 1703–1715.e1737 (2019).
50. Silva, N. J. et al. Inflammation and matrix metalloproteinase 9 (Mmp-9) regulate photoreceptor regeneration in adult zebrafish. *Glia* **68**, 1445–1465 (2020).
51. Chuang, H. C., Wang, X. & Tan, T. H. MAP4K Family Kinases in Immunity and Inflammation. *Adv. Immunol.* **129**, 277–314 (2016).
52. Kastan, N. et al. Small-molecule inhibition of Lats kinases may promote Yap-dependent proliferation in postmitotic mammalian tissues. *Nat. Commun.* **12**, 3100 (2021).
53. Kastan, N. R. et al. Development of an improved inhibitor of Lats kinases to promote regeneration of mammalian organs. *Proc. Natl. Acad. Sci. USA.* **119**, e2206113119 (2022).
54. Zhang, S. & Zhou, D. Role of the transcriptional coactivators YAP/TAZ in liver cancer. *Curr. Opin. Cell Biol.* **61**, 64–71 (2019).
55. Li, F. L. & Guan, K. L. The two sides of Hippo pathway in cancer. *Semin. Cancer Biol.* **85**, 33–42 (2022).
56. Toda, R., Kawazu, K., Oyabu, M., Miyazaki, T. & Kiuchi, Y. Comparison of drug permeabilities across the blood-retinal barrier, blood-aqueous humor barrier, and blood-brain barrier. *J. Pharm. Sci.* **100**, 3904–3911 (2011).
57. Wang, L. & Zhang, H. Ocular barriers as a double-edged sword: preventing and facilitating drug delivery to the retina. *Drug Deliv. Transl. Res.* **13**, 547–567 (2023).
58. Ndubaku, C. O. et al. Structure-Based Design of GNE-495, a Potent and Selective MAP4K4 Inhibitor with Efficacy in Retinal Angiogenesis. *ACS Med. Chem. Lett.* **6**, 913–918 (2015).
59. Anastassiadis, T., Deacon, S. W., Devarajan, K., Ma, H. & Peterson, J. R. Comprehensive assay of kinase catalytic activity reveals features of kinase inhibitor selectivity. *Nat. Biotechnol.* **29**, 1039–1045 (2011).
60. Gao, Y. et al. A broad activity screen in support of a chemogenomic map for kinase signalling research and drug discovery. *Biochem. J.* **451**, 313–328 (2013).
61. Roska, B. & Sahel, J. A. Restoring vision. *Nature* **557**, 359–367 (2018).

ACKNOWLEDGEMENTS

This work was supported by grants from the National Key R&D Program of China (No. 2018YFA0107304, Z.L., No. 2018YFA0107301, W.L., No. 2019YFA0111200, Y.L.), National Natural Science Foundation of China (No. 81870627, Z.L.; No. U20A20363, J.H.). S.J.F. is the recipient of a Research Career Scientist (RCS) Award (I K6 BX005787) from the Department of Veterans Affairs, BLR&D Service. The opinions expressed herein do not reflect those of the Department of Veteran Affairs or any agency the

U.S. Government. We thank Dr. Zhen Liu for providing the MIO-M1 cell line. We thank Jingru Huang and Xiang You from Central Lab, School of Medicine, Xiamen University for technical support in confocal imaging. We thank Caiming Wu (State Key Laboratory of Cellular Stress Biology, School of Life Sciences, Xiamen University) for help with droplet digital PCR. We thank Haiping Zheng from Central Lab, School of Medicine, Xiamen University for technical support in fluorescence-activated cell sorting (FACS). We also thank Dr. Wenjun Xiong from Hongkong City University, Dr. Dan Du from Xiamen University, Dr. Kuan Zhang from Army Medical University and Dr. Huaxi Xu from Xiamen University for insightful suggestions and discussions.

AUTHOR CONTRIBUTIONS

Z.L., Y.L., and H.Z. designed the overall project; H.Z., Y.G., Y.L., J.H., W.L., and S.J.F. wrote/edited the manuscript; H.Z. and Y.G. performed most of the experiments and data analysis. Y.Y. screened and identified Glast-CreERT2 + /tg; ROSA26R-tdTomato + /tg mice for tracing experiment. J.W. provided $Yap^{flox/flox}$ mice for YAP knockout experiments. H.X. provided Glast-CreERT2 + /tg mice and useful discussions. Y.Z. and S.L. performed the electrophysiological (ERG) analyses. Y.Q. helped to perform the drug delivery in vivo. J.Z., Y.W., Y.Z., M.S., J.Z., and R.Z. performed partial real-time PCR, Western blot and immunofluorescence analyses. H.Z. and Y.G. contributed equally to this work, thus should be considered as co-first authors. All authors read and approved the final manuscript.

COMPETING INTERESTS

The authors declare no competing interests.

ADDITIONAL INFORMATION

Supplementary information The online version contains supplementary material available at https://doi.org/10.1038/s41536-023-00310-6.

Correspondence and requests for materials should be addressed to Yi Liao or Zuguo Liu.

Reprints and permission information is available at http://www.nature.com/reprints

Publisher's note Springer Nature remains neutral with regard to jurisdictional claims in published maps and institutional affiliations.